Palaeontological framework from Pirabas Formation (North Brazil) used as potential model for equatorial carbonate platform

Orangel Aguilera, Olga M. Oliveira de Araújo, Austin Hendy, Anna A.E. Nogueira, Afonso C.R. Nogueira, Clovis Wagner Maurity, Vinicius Tavares Kutter, Maria Virgínia Alves Martins, Giovanni Coletti, Bruna Borba Dias, Silane A.F. da Silva-Caminha, Carlos Jaramillo, Karen Bencomo, Ricardo Tadeu Lopes

PII: S0377-8398(19)30113-6

DOI: https://doi.org/10.1016/j.marmicro.2019.101813

Reference: MARMIC 101813

To appear in: *Marine Micropaleontology*

Received date: 12 August 2019

Revised date: 4 December 2019

Accepted date: 4 December 2019

Please cite this article as: O. Aguilera, O.M. Oliveira de Araújo, A. Hendy, et al., Palaeontological framework from Pirabas Formation (North Brazil) used as potential model for equatorial carbonate platform, *Marine Micropaleontology*(2019), https://doi.org/10.1016/j.marmicro.2019.101813

PALAEONTOLOGICAL FRAMEWORK FROM PIRABAS FORMATION (NORTH BRAZIL) USED AS POTENTIAL MODEL FOR EQUATORIAL CARBONATE PLATFORM

Orangel Aguilera[1], Olga M. Oliveira de Araújo [2], Austin Hendy[3], Anna A. E. Nogueira[4], Afonso C. R. Nogueira[4], Clovis Wagner Maurity[4], Vinicius Tavares Kutter[4], Maria Virgínia Alves Martins[5,6,] Giovanni Coletti[7], Bruna Borba Dias[1], Silane A. F. da Silva-Caminha[8], Carlos Jaramillo[9,10], Karen Bencomo[1], Ricardo Tadeu Lopes[2],

[1]Fluminense Federal University (UFF), Paleoecology and Global Changes Laboratory, Campus Gragoatá, Bloco M, No. 110, CEP: 24210-200, Niterói, Rio de Janeiro, Brazil. e-mail: orangel.aguilera@gmail.com; brunaborbadias@id.uff.br; karen.karess@gmail.com

[2]Federal University of Rio de Janeiro (UFRJ), Nuclear Instrumentation Laboratory, Nuclear Engineering Program/COPPE, Rio de Janeiro, Av. Horácio Macedo, Cidade Universitaria, 21941-450, Brazil. e-mail: olgaufrj.lin@gmail.com; ricardo@lin.ufrj.br

[3]Natural History Museum of Los Angeles County. 900 Exposition Blvd, Los Angeles, California, USA. e-mail: ahendy@nhm.org

[4]Federal University of Para (UFPA), Geoscience Institute, Belém, Pará, Brazil. e-mail: bioanna@gmail.com; anogueira@ufpa.br; clovis.maurity@gmail.com; viniciuskutter@id.uff.br

[5]Rio de Janeiro State University (UERJ), R. São Francisco Xavier, 524 - Lab 1006 - Maracanã, Rio de Janeiro, 20550-900, Brazil. e-mail: virginia.martins@ua.pt

[6]Aveiro University, Department of Geoscienses, GeoBioTec, Campus de Santiago, 3810-197, Aveiro, Portugal.

[7] University of Milano Bicocca, Department of Environmental Sciences and Earth Sciences, Piazza della Scienza 4, 20126 Milano, Italy. e-mail: giovanni.coletti@unimib.it

[8] Federal University of Mato Grosso (UFMT), Paleontology and Palynology Laboratory, Cuiabá, Mato Grosso, Brazil. e-mail: silane.silva@gmail.com

[9] Smithsonian Tropical Research Institute, Balboa, Ancon, Panamá. email: JaramilloC@si.edu

[10]ISEM, U. Montpellier, CNRS, EPHE, IRD, Montpellier, France

Abstract

The Pirabas Formation (early to middle Miocene) from the equatorial margin of North Brazil is characterized by a shallow-marine carbonate platform with high fossil diversity and abundant micro- and macrofossil remains. The Pirabas Formation represents a unique carbonate system along the Atlantic margin of South America that developed before the onset of the Amazon delta. We studied the paleontology and lithofacies of outcrops of the uppermost Pirabas Formation and found that was deposited in a coastal marine environment with marginal lagoons under the influence of a tidal regime and tropical storms. The remains of calcareous algae, molluscs, crustaceans, echinoderms, bryozoans, solitary corals, fish and marine mammals, together with foraminifera, ostracods and other marine microfossils, shaped a biogenic framework, that together with the post-depositional processes of dissolution of skeletal grains, is responsible for the mean packstone-floatstone porosity of 14.9%. The palaeontological framework and the petrophysical characterization of the carbonate rocks from the uppermost Pirabas Formation outcrop represent a baseline to interpret the entire Pirabas Formation in the subsurface stratigraphic sections (cores) of this important Neogene unit. Considering that carbonate rocks account for ~50% of oil and gas reservoirs around the world, this research provides a model for Neogene tropical carbonate deposits useful for carbonate petroliferous reservoirs in the Brazilian equatorial basins.

Keywords: Marine Fossil, Western Atlantic, Miocene, Carbonate Platform, Micro CT

1. Introduction

The carbonate platform in the equatorial margin of North Brazil (Soares et al., 2011) includes the Foz do Amazonas Basin (Figueiredo et al., 2007), Pará-Maranhão Basin (Soares et al., 2007) and Barreirinhas Basin (Trosdtorf-Junior et al., 2007) in the coastal plain of the states of Pará and Maranhão. Oligocene-Miocene circumtropical carbonate deposits have similar stratigraphic characteristics across tropical America (Leigh et al., 2013), Asia (Vahrenkamp, 1998; Zampetto et al., 2003; Janjuhah et al., 2017a; Dill et al., 2018), Africa (Buchbinder, 1996; John et al., 2003) and Australia (Ehrenberg et al., 2006), and most of these Cenozoic carbonate sequences are potential reservoirs for gas and oil exploration.

Miocene carbonate deposits from northern Brazil are exposed along the onshore coastal plain of Pará State and are represented by the Pirabas Formation (Maury, 1925). The Pirabas Formation accumulated in a western Atlantic shallow-marine setting until carbonate production was terminated as consequence of the massive imput of siliciclastic sediments from both the Amazon delta and the coastal plain drainages during the late Miocene (Damuth and Kumar, 1975; Wolff and Carozzi, 1984; Brandão and Feijó, 1994; Silva et al., 1998; Figueiredo et al., 2009; Watss et al., 2009). Andean alluvial terrigenous sediments (Hoorn et al., 2017) filled the Marajó Basin following the progradation of the Barreiras Formation which overlaps the Pirabas carbonates (Rossetti et al., 2013; Aguilera et al., 2017b).

The Pirabas Formation outcrops, first studied by Ferreira-Penna (1876), have a high density and diversity of fossils. White (1887) and Maury (1925) conducted the first studies of the mollusc, bryozoan, and coral assemblage from this formation. Palaeontological contributions by Petri (1957) on foraminifera, Beurlen (1958 a, b) on crustaceans, Santos

(1958, 1967) on echinoids, Barbosa (1961) on bryozoans, Fernandes (1979, 1981) on corals, Santos and Travassos (1960) on fish, Paula-Couto (1967) on sirenids, and Duarte (2004) on the palaeoflora further improved the knowledge of the Pirabas Formation. Additional contributions included new species descriptions and new records compiled by Távora et al. (2010), Aguilera and Páes (2012), Aguilera et al. (2013 a, b, c; 2014; 2017 a, b) and palaeontological reviews of bryozoans (Távora et al., 2014; Zágoršek et al., 2014; Ramalho et al., 2015, 2017; Muricy et al., 2016), echinoids (Mooi et al., 2018) and ostracods (Nogueira and Nogueira, 2017). Palaeoclimatic interpretations based on taphoflora show mean annual atmospheric temperatures ranging between 24.6 °C and 25.0 °C and mean annual precipitation between 1,849 and 2,423 mm (Santiago and Ricardi-Branco, 2018). Isotopic analyses of teeth from fossil elasmobranchs (derived $\delta^{18}O$ temperature) indicated a mean seawater palaeotemperature of 26.3 °C, ranging between 21.7 °C and 30.1 °C (Aguilera et al., 2017a). Both terrestrial palaeoclimate and the ocean palaeotemperatures could be related to the final stages of an abrupt episode of global cooling at the Oligocene-Miocene boundary, the Mi-1 glaciation (Stewart et al., 2017; Egger et al., 2018) and the global warming period of the middle Miocene climate maximum (You et al., 2009; Goldner et al. 2014).

In spite of the abundant and excellent preservation of the fossil record in the Pirabas Formation, palaeontological research in the Pirabas Formation over the past two decades has been scarce, isolated, and restricted to outcrop surveys and has produced doubtful taxonomic identifications (e.g., see Muricy et al., 2016 for bryozoans; Luque et al., 2017 for crustaceans). Furthermore, both the stratigraphic framework of the carbonate deposits and the influence of diagenesis on the carbonate porosity remain unknown.

The main aims of this work are to provide an accurate description of the biogenic framework of carbonate rocks, detailed palaeoenvironmental interpretation, palaeontological assemblage descriptions and a stratigraphic facies model for Pirabas Formation. We used a wide arrange of tools in multiple scientific fields to reach accurate palaeoenvironmental results using high technological resources and innovative solutions in the field of micropalaeontology. The new dataset acquired by microcomputer tomography (CT) allow high-resolution recovery of fossil arrangement in the matrix and can provide an important baseline for core research on analogous equatorial Brazilian carbonate platforms.

2. Geological setting

The Pirabas Formation is located in the northeastern area of Pará State, Brazil (Fig. 1). It represents an early to middle Miocene marine unit of the Bragantina Platform (Rossetti et al., 2013). The Pirabas Formation has been described as representing a complex inshore shallow platform (consolidated grainstones and packstones, stratified wackestone to laminate packstones and mudstones). Coastal palaeoenvironments (shoreface/foreshore deposits), marginal lagoons, restricted platforms (grey to olive green mudstones and conglomerate sandstones) and estuarine mangroves (dark and laminated mudstones) are also found in the Pirabas (Góes et al., 1990; Rossetti, 2001; Rossetti and Góes, 2004; Rossetti et al., 2013; Aguilera et al., 2013 a, b; Borges, 2016). Three major ecofacies have been described, the Capanema Ecofacies (lagoonal environment), the Baunilha Grande Ecofacies (open marine, lagoon, and mangrove forest environments) and the Castelo Ecofacies (continental and carbonate platform environments) (Antonioli et al., 2015 and references therein). Early studies suggested that the Capanema is the oldest ecofacies and it is overlain by the Baunilha Grande Ecofacies, which in turn is overlain by the Castelo

Ecofacies, the top of the Pirabas Formation (Francisco et al., 1971). The Castelo Ecofacies is overlain by the Barreiras Formation, a fully siliciclastic unit (Francisco et al., 1971; Antonioli et al., 2015 and references therein). Later works highlighted that these three ecofacies are interlayered rather than stacked, with gradual lateral and vertical facies transitions (Ferreira and Francisco 1988; Antonioli et al., 2015 and references therein). The Baunilha Grande Ecofacies was dated to be in palynological zone T-13, 17.7 to 16.1 Ma (late Burdigalian), of Jaramillo et al. (2011), using samples from the locality of Quatipuru (about 50 km ovest of Salinopolis) (Antonioli et al., 2015).

The majority of the published studies on the Pirabas Formation have been mostly restricted to few stratigraphic metres at outcrops and quarries (Góes et al., 1990; Leite, 2004; Rossetti and Góes, 2004; Aguilera and Paes, 2012; Rossetti et al., 2013; Borges, 2016), while the rest of the formation, measuring almost 148 m (Freimann et al., 2014), still remains unknown. There are many controversies over its age, its facies framework and how it correlates to contiguous, coeval and analogous Brazilian equatorial carbonate platforms of the Amazon Basin (e.g., Amapa Formation: Schaller et al., 1971), Pará-Maranhão Basin (e.g., Ilha de Santana Formation: Pamplona, 1969; Abreu et al., 1986) and Barrerinhas Basin (e.g., Pirabas Formation: Maury, 1925; Pamplona, 1969). Planktonic foraminiferal assemblages (Petri, 1954, 1957; Ferreira et al., 1978; Fernandes, 1984, 1988; Fernandes and Távora, 1990; Távora and Fernandes, 1999) and palynomorphs (Leite, 2004) mainly suggest an early to middle Miocene age, zones N5 to N8 of Berggren et al. (1995), corresponding to zones M2 to M5 of Wade et al. (2011) (late Aquitanian to early Langhian). This age overlaps the palynological data from the Atalaia outcrop (Silva, 2016) and Capanema B-17 Quarry (Aguilera et al., 2014). Nogueira and Nogueira (2017) suggest an Oligocene-Miocene age based on ostracod assemblages, while Martinez et al. (2017),

based on isotopic analyses of 87Sr/86Sr from molluscs, suggested an early Miocene Burdigalian age (17.3 to 16 Ma).

3. Materials and methods

Field trips to the Pirabas Formation were conducted during low tides at the Atalaia beach outcrop, Salinópolis municipality (0º 35' 37" S, 47º 18' 54.4" W), Pará State, Brazil. A ~5 meter stratigraphic section at Atalaia was mapped and measured (Fig. 1). The stratigraphic location of Atalaia seems to be at the very top of the entire Formation, just below the contact with the overlying Barreiras formation. Rock samples were collected vertically along the section from the base (0.10 m) to the top (5.0 m), using a masonry saw to cut out large pieces of slabs (six slabs at 3.9 m and five slabs at 5.0 m), portable drill to cutting out micro plugs (two plugs at 5.0, 4.5, 3.9, 3.6 and 2.8 m from each level; one plug at 0.4 and 0.3 m from each level; two plugs at 0.1 m), acrylic tube core to collect unconsolidate samples including one core per level at 3.0, 2.5 and 2.4 m, and a bulk with six kilograms of samples at 3.4 m. (Fig. 2).

Micro-CT was performed on all rock pieces (slabs) with sizes of approximately 190 mm long, 80 mm high and 30 mm wide were using a V/TOMEX/M (GE) instrument (Fig. 3). All micro plugs approximately 60 mm in length and 25mm in diameter were also used for nanno-CT acquisition (Fig. 4). Each single micro plug used for the nanno scanner represented three thousand 3D sections (X, Y, Z) with detailed views of the microfossil framework (Supplementary file S1). The micro-CT parameters for the acquisition of these large slices included a current of 150 KV, an energy of 350 µA, 5 frame, and a Cu filter with a thickness of 0.3 mm. The geometry had a magnification of 24.94, pixel size of 10.47 µm, FOD of 43.37 mm and FDD of 807.68 mm. The pixel size during the rotation step 0.5°

to 360° along the Z-axis of samples was 18 µm. The 3D volume was reconstructed using the software Phoenix Datos/X reconstruction v. 2.2 (GE), and for visualization VG Studio v. 3.0. Subsamples (micro plugs) of ~3000 mm^3 were used for nanno-CT microfossil acquisition. In order to calibrate the images we used a four-step process including, (i) alignment, (ii) smoothing, (iii) X-ray spectra attenuation and (iv) correction of ring artifacts. The procedures of image segmentation for rocky matrix and for pore mesh were used to obtain separate quantitative analyses. The micro-CT analyses included (i) the identification of fossil assemblages on the rocky matrix, (ii) the thickness of the rocky matrix and pore separation, (iii) the total porosity. Reconstructed 3D models of fossil fauna were used for systematic palaeontological identification (Figs. 5-7, 11), following three steps: (i) identification and digital selection of the fossil structure along the acquisitions sets, (ii) separation of the volume of interest of the recovered fossil using the software CT-Analyzer v 3.1, (iii) construction of 3D models of fossils using the Avizo Fire 9.1, and (iv) digital editing of composite images using Photoshop S5.

We used Digital Rock Physics for fast-forward imaging technology to predict the petrographic properties (such as porosity). The petrographic analysis was performed using CT-Analyzer v.3.1. The morphometric porosity analyses followed the image discretization of elements as a function of the grey level; the pore volume was identified by the black pixels in the images and separated from the grey level pixels as the rock matrix. We used the global segmentation method compiled by De Araújo et al. (2018) to separate the images into two categories (background and object). This separation was accomplished by scanning an image peer to peer and identifying the elements as points of the object or background according to a threshold. Thus, a binary image was obtained with the objects in black (0) and the background in white (255) following the Gonzales and Woods (2002)

method. This technique allowed to separate the porosity of the carbonate rock and to calculate the quantitative results for the total porosity (%), the number of pores per slice and the pore size distribution.

Twelve thin sections of subsamples (six at 3.9 and five at 5.0 m) were prepared for petrographic analysis, fixed to 76×26 mm glass slices and polished to 30 µm thickness. The photomicrographs were obtained using a petrographic microscope with an integrating digital system (Figs. 8-10, 12-13). A photomosaic was acquired from each petrographic slice using a motorized petrographic microscope. From each slice, we use a set of parallel acquisition modes (Module P&B) and crossed acquisition modes (Pol TL) with a 10X objective. The compositions of the skeletal assemblages were also studied on thin sections using the point-counting technique and more than 300 points were counted in each section (Flügel, 2010). The palynological slides from the Atalaia outcrop, described in Leite (1997) under the numbers GP/4E 1453 to 1461, are deposited in the palynological collection of the University of São Paulo. These slides were reanalysed in order to infer age and to compare them with new assemblages described in northern Amazonia (Jaramillo et al., 2011). The entire bulk samples were processed and sieved at the laboratory using 500 µm, 250 µm, 125 µm and 63 µm mesh sizes. The photomicrographs of specimens were made using light stereomicroscopy with an integrating digital system and using a scanner electron microscope for selected specimens. All rock slices and micro plugs were deposited in the Palaeoecology and Global Changes Laboratory (LP&MG) at Fluminense Federal University, Niterói, Rio de Janeiro.

4. Results

4.1. Age

The co-occurrence of palynomorphs *Crassoretitriletes vanradshoovenii*, *Psilastephanocolporites tesseroporus* and *Malvacipolloides maristellae* (Figs. 14.1, 14.11 and 14.10, respectively) (Leite, 1997; Antonioli et al., 2015; Silva, 2016), indicates a middle Miocene age (palynological T15 zone, 14.2 – 12.7 Ma, late Langhian to Serravallian; Jaramillo et al., 2011) for the top of the Pirabas Formation at the Atalaia outcrop. Common species of mangroves such as *Zonocostites ramonae*, *Lanagiopollis crassa* and *Deltoidospora adriennis* (Figs. 14.3-14.4, 14.5-14.7 and 14.22, respectively) are abundant in the palynological records but cannot be used to date those outcrops due to their long-range stratigraphic distributions (Leite, 1997; Aguilera et al., 2014; Antonioli et al. 2015; Silva, 2016).

Identifications of foraminifera from the lithified layer of the Atalaia outcrop, using micro-CT and 3D reconstruction, include species of the families Hauerinidae (*Pyrgo*, *Quinqueloculina*, *Spiroloculina*) and Milamminidae (*Spirosigmoilinella*). In addition, identifications from the petrographic slices include Amphisteginidae, Elphidiidae, Globigerinidae, Miliolidae, Soritoidea and Textulariidae. The samples from the poorly lithified layers yielded the species *Ammonia parkinsoniana*, *Amphistegina lessonii*, *Elphidium sagrum*, *Guttulina ovalis*, *G. irregularis*, *Guttulina* sp., *Planulina* sp., and *Pyrgo subsphaerica*. The majority of these species have a very long stratigraphic range and do not offer information to date the formation. However, the apparent absence of *Lepidocyclina* in the Atalaia outcrop samples (which disappears from the American bioprovince in the Burdigalian; BouDagher-Fadel and Price, 2010), could be consistent with a post-Burdigalian age for Atalaia.

4.2. Lithology and microfacies

The composite section of the Atalaia outcrop is five meters long. It is overlain by the siliciclastic sandstones and mudstones of the Barreiras Formation, while the contact with the underlying basement was not observed as the Pirabas formation is ~148 meters thick (Fig. 1). Four main lithologies can be observed in the outcrop. Massive yellowish packstone to floatstone with a diverse fossiliferous assemblage, including disarticulated macrofossils, fragmented shells, mollusks moulds (including common specimens of the gastropod *Turbinella*) and vertebrate remains. The siliciclastic fraction of this rock is dominated by sand-sized quartz grains (sub-rounded to sub-angular) and opaque minerals (mainly Fe2O3) (Fig. 1). Dark-green, poorly consolidated wackstone with foraminifera, ostracods, echinoderms fragments and common grains of quartz (sub-rounded to sub-angular) (Fig. 1). Dark-green massive dolomudstone, without well preserved macrofossils, characterized by a dolomite-matrix and with common grains of quartz (Fig. 1). Fossiliferous and locally bioturbated dark mudstones (Fig. 1).

On the basis of the fossiliferous content three main microfacies (A, B, C) were recognized, corresponding to different coastal environments. The Microfacies A which characterizes the packstone to floatstone layers and presents a skeletal assemblage dominated by large benthic foraminifera (mostly soritids) and molluscs. Echinoderm remains and coralline algae are also common, while *Halimeda* plates, bryozoans and small benthic foraminifera are less abundant (Figs. 8-10, 12-13). Vertebrates remains (including bones of sirenids and shark teeth) also occur. In this facies, due to the high porosity, aragonite shells (e.g., gastropods and solitary corals) are mostly dissolved during the early phase of diagenesis, forming empty vugs and moulds that are often infilled by calcite (Figs. 2, 3); micritized fragments of fossils are also present. Microfacies A seems to have accumulated in a shallow inner platform located in the shallowest part of the photic zone, as

suggested by the abundance of soritids and the presence of green calcareous algae. The abundance of epiphytic foraminifera (the soritids in particular) suggests the presence of a vegetated substrate, possibly a seagrass meadow. Microfacies B characterizes the poorly consolidated wackstones, it presents a skeletal assemblage dominated by echinoderms (mainly crinoids, ophiuroids and asteroid ossicles, echinoid test fragments and spines), benthic foraminifera (mostly *Amphistegina lessonii*, *Ammonia parkinsoniana* and *Elphidium sagrum*; Fig. 15) and ostracods. Bryozoans, fragments of the carapace and chela of decapods, shark teeth and otoliths also occur. The palaeoenvironment of microfacies B is interpreted as a surf zone, where very small fragments of marine organisms randomly accumulated. Microfacies C characterizes the fine grained rocks of the central part of the interval (the mudstone and the dolomudstones). The skeletal assemblage includes echinoderms, crustaceans remains (including whole specimens buried in their tunnels) and plant remains (including pyritized trunks). This microfacies is probably related to a protected lagoonal setting, with the dolomite-rich layers possibly related to a tidal-flat environment and the dark mudstones related to a brackish, dysoxic, environment, possibly related to a mangrove forest.

4.3. Fossil assemblages and palaeoecology

The fossil record of the Atalaia outcrop shows a wide diversity of taxa including plants, calcareous algae, foraminifera, ostracods, sponges, bryozoans, corals, molluscs, echinoderms, crustaceans, fish and sea mammals that seems to have accumulated in shallow tropical marine palaeoenvironment (inner platform, from the tidal zone to water depths of less than 50 m) (Fig. 17). Foraminifera are characterized by the common occurrence of shallow continental-shelf species *Amphistegina lessonii* (most abundant

species in the poorly consolidate wackstone) and *Guttulina ovalis* (Birkenmajer and Jednorowska, 1997), followed by *Elphidium sagrum*, *Elphidium poeyanum* and *Ammonia parkinsoniana*, which are indicative of warm and low-salinity waters, according to Petri (1954). The abundant presence of soritids, observed in the thin sections of the packstone to floatstone, also suggests a shallow marine setting (Murray, 2006). The combination of large benthic epifaunal species (*Amphistegina* and soritids) together with small miliolids (such as *Pyrgo* and *Spiroloculina*), brackish and/or stress-tolerant species (*Ammonia parkinsoniana*, *Elphidium sagrum*, *Spirosigmoilinella*) and rare planktonic organisms is generally considered indicative of shallow coastal settings (inner shelf/back reef/lagoonal/transitional) both in modern oceans and in the Neogene (Culver, 1988; Reid 1998; Leckie and Olson, 2003; Fiorini and Jaramillo 2007; Boudagher-Fadel, 2008; Hayward, 2014; Zoeram et al., 2015; Mir et al., 2017; Roozpeykar et al., 2019).

The distribution of the microfacies along the section could suggests a major environmental cycle starting with inner-platform conditions (A), moving into shoreface condition (B), then into a restricted lagoonal environment (C) and then back again to shoreface and inner-platform conditions (Fig. 1). The abrupt lithological changes observed in such a short section could be related to brief periods of exposure and or depositional/erosive cycles, possibly resulting in massive mortality in the benthic fauna and floral assemblages.

4.4. Fossil preservation

Aragonite shells and corals were mostly dissolved during diagenesis followed by calcite recrystallization and cementation especially in low-energy palaeoenvironments where high organic contents favoured microbial decay and acidity. We observed frequent shell remains

of juvenile and adult gastropods, such as *Turbinella* cf. *tuberculatus* (Ferreira, 1964), and bivalves, such as *Mercenaria* sp., that were lost due to the dissolution of the entire hard shell and are preserved exclusively as internal moulds infilled by packstone matrix. In the wackstone, the preservation of shells is very rare and mostly represented by micro molluscs. In contrast, the bryozoans are fragmented but well preserved. The high-Mg calcite skeletons of echinoderms (crinoids, ophiuroids and echinoids) are thermodynamically metastable (Kroh and Nebelsick, 2010), but still more stable than aragonitic remains and this explain the better preservation of these biogenic fragments. Disassociated siliceous spicules of sponges are also well preserved. Unlike mangrove derived-pollen, benthic foraminifera typical of mangrove environments were not observed. Generally, the benthic foraminifera assemblage in mangroves is mainly composed of agglutinated species with low preservation potential due to post-mortem disaggregation (Woodroffe et al., 2005). Furthermore, in the mangrove forest environment, the acids released from organic material remineralization are not favourable for the preservation of most foraminiferal taxa (Woodroffe et al., 2005; Wilson and Vicent, 2014). Presently, an extant mangrove area near Atalaia presents a foraminiferal assemblage dominated by species from the genera *Arenoparrella*, *Haplophragmoides* and *Trochammina* (Laut et al., 2010), which might have also inhabited the area during the Miocene.

4.5. Pirabas assemblage and taphonomy

The arrangement of biogenic remains in Microfacies A and B (disarticulated and fragmented shells, broken echinoderms tests and spines, fragments of branched, encrusting and free-living bryozoans, fragments of coralline red algae, *Halimeda* and large benthic foraminifera) in a cemented carbonate matrix could be related to a marine environment

with strong currents (probably of tidal origin) affecting a complex system of coastal environments (Longhitano et al., 2012). The extremely broken shells and heavily fragmented echinoid tests (Figs. 2.2-2.5, 4) could be a consequence of strong littoral currents and high wave energy in the surf zone and/or tropical storms. Entire specimens of molluscs and echinoids recovered in "living position", and decapod crustaceans buried in their galleries (the latter in microfacies C) could be interpreted as representing rapid burial events. Empty molluscs covered by boring sponges, encrusting bryozoans and balanoids fixed over shells reflect the dynamic use of available substrates for colonization (Figs. 5.1, 5.2, 5.16, 6.8).

4.6. Porosity

Primary pores (depositional porosity) are represented by interparticle and intraparticle pores within fragments of calcareous algae, foraminifera, bryozoans, echinoderms, and mollusc shells. Secondary pores, which are those resulting from carbonate dissolution during depositional diagenesis, consist of large empty moulds in the rock matrix (Figs. 3, 4, Appendix S1). The cementation, associated with the mechanical or chemical compaction, results in a mean packstone-floatstone porosity of 14.93% (n=7), wackstone 2.64% (n=1), dolomustone 1.4% (n=1) and dark mudstone 0.97% (n=2). Overall, the five meters section of the Atalaia outcrop has low porosity (Figs. 1, 18-19) compared with desirable porosity values above 25% for an oil reservoir (Sadeq and Yusoff, 2015).

5. Discussion

5.1. Context and correlations with coeval units of tropical carbonate deposits

Oligocene-early Miocene biogenic carbonate deposits in tropical regions are commonly produced by coralline red algae, large benthic foraminifera and bryozoans (e.g., Malta: Brandano et al., 2009; Brazil: BouDagher-Fadel et al., 2010, Sousa et al., 2003; India: Sarkar et al., 2016; Iran: Roozpeykar and Moghaddam, 2016 and Allahkarampour et al., 2018; France: Coletti et al., 2017, 2018; Italy: Brandano and Corda, 2002, Coletti et al., 2017) or by hermatypic corals and coralline algae (e.g., western Mediterranean: Braga et al., 2009; eastern Mediterranean: Coletti et al., 2019; Malaysia: Mihaljevic et al., 2014; Janjuhah et al., 2017a).

At the top of the Pirabas Formation at Atalaia outcrop, there is no evidence for large coral reef deposits (Fig. 1). In the shallow water palaeoenvironments of the equatorial Oligocene-Miocene Brazilian carbonate platform (e.g., Pará-Maranhão Basin: Abreu et al., 1986), there is no record of large scleractinian coral reefs, and the coral fauna is mainly dominated by isolate ahermatypic Flabellidae, as in the Pirabas Formation. Flabellids are exclusively solitary and distributed worldwide from neritic to abyssal occurrences, including cold-water species recorded in Antarctic, sub-Antarctic, southwest Atlantic and south Pacific waters (Scheltser and Bremec, 2015). The upper Pirabas Formation differs from the modern optimal range for coral reef production. The relatively high terrestrial run-off, testified by the presence of abundant quartz grains, was probably sufficient to reduce water transparency and hinder the development of coral reefs, similar to the equatorial Spermonde Shelf, which is characterized by reduced water transparency and significant terrestrial run-off (Wilson and Vecsei, 2005). On the other hand, large benthic foraminifera (and in particular *Amphistegina*, which is the most common genus in Microfacies B) and coralline algae are more tolerant than hermatypic corals to high nutrient concentrations, high sedimentation sedimentation rate, reduced water transparency and abrupt temperature

variations (Langer and Hottinger, 2000; Langer, 2008; Lokier et al. 2009; Mateu-Vicens et al. 2009; Coletti et al., 2017). The stressful, shallow-water coastal environment of the uppermost Pirabas Formation was probably more suited for the development of mangrove forests and seagrass meadows rather than fringing coral reefs. The abrupt episode of global cooling near the Oligocene-Miocene boundary (Mi-1: 23.0 Ma; Stewart et al., 2017), which led to the early Miocene coral reef extinction in tropical America and removed up 50% of late Oligocene diversity (Johnson et al., 2009), together with eustatic sea level changes (Haq, 1987; Kominz et al., 2008), was also a strong limiting factor for the development of coral reefs in the region. These palaeoenvironmental changes could also have favoured calcareous algae, seagrass, and associated shallow water faunal assemblage, as testified by their expansion throughout the stratigraphic sequences of the Amapá, Ilha de Santana and Pirabas formations along the equatorial margin of Brazil.

5.2. Pirabas Sea and the late Oligocene-early Miocene stratigraphic hiatus

Sections of the Amapá Formation (Foz do Amazonas Basin: Schaller et al., 1971), Ilha de Santana Formation (Pará-Maranhão Basin: Pamplona, 1969; Abreu et al., 1986) and Pirabas Formation (recorded in the Barreirinha Basin: Pamplona, 1969) in the equatorial platform of Brazil show an Oligocene-Miocene hiatus interpreted by Abreu et al. (1986) as an erosive phase without deposition. This hiatus could also be a consequence of sea level oscillation (Haq, 1987; Kominz et al., 2008) and the Mi-1 event (Stewart et al., 2017; Egger et al., 2018). In the outcrops of the Pirabas Formation, the hiatus recorded in the Foz do Amazonas, Pará-Maranhão and Barreirinha basins was not observed because only a few meters of onshore section are available for accurate interpretation. However, the seismic records of palaeocanyons in the Pará-Maranhão Basin support the Oligocene-Miocene

subaerial erosive phase on the carbonate platform recorded by Abreu et al. (1986). The abrupt lithological changes observed in the Atalaia section could be related to brief periods of exposure and or minor erosive phases. Climate and weathering were favourable for erosion and fast diagenesis. In addition, deposits of siliciclastic material throughout the fluvial drainage and the transport of continental debris (e.g., palaeoflora: *sensu* Santiago and Ricardo-Branco, 2018) to the marine deposits of the Pirabas Formation show the complexities of these outcrops. The coastal plain dominated by mangrove forests in the Baunilha Grande locality (*sensu* Antonioli et al., 2015) is an example of habitat lost during the abrupt burial of infauna (e.g., *Uca maracoanai antiqua* Brito, 1972).

5.3. Porosity characterization

The fossil framework and bioclastic arrangement, meteoric leaching, cementation, depth of burial and pressure of compaction are related factors responsible for the total porosity and permeability of carbonate platform deposits (Schmoker and Halley, 1982; Hébert et al., 2014; Rashid et al., 2015; Sadeq and Yusoff, 2015; Janjuhah et al., 2017b). The heterogeneity of pore structures, especially in the Atalaia outcrop of the uppermost Pirabas Formation, is already visible at the centimeter scale in the coquinoid packstone to floatstone layers from the top at 5.0 m (16.61% porosity; Figs. 1, 18) to the base at 0.1 m (9.91% porosity; Figs. 1, 19). The packstone to floatstone horizons affected by strong diagenetic processes, exemplified by the *Turbinella* and *Mercenaria* basal horizon (0.10 m), show the lowest porosity for this lithology (approximately 10%). These porosity values are similar to those of South Florida carbonates analysed by Schmoker and Halley (1982). The range of the values is also similar to those of other shallow-water, low-latitude, marine carbonates. According to Vasconcellos (2013), in the middle Miocene Pirarucu Formation from the Fóz

de Amazonas Basin in Brazil, the total porosity ranges between 23 and 27% (well: 1 APS 0010B AP). However, in the early Palaeocene to middle Miocene Amapá Formation in the Fóz do Amazonas Basin, the total porosity ranges between 12 and 18% (well: 1APS 0021 AP). The porosity of carbonate strata cored on the Marion Plateau (early to late Miocene), offshore from northeastern Australia (Ehrenderg et al., 2006) ranges between 5 and 55% (overview of limestone, dolostone and partly dolomitized plugs data).

5.4. The collapse of the carbonate platform

The equatorial margin of Brazil is a stable platform not affected by the Cenozoic Caribbean and Andean orogenies (Almeida et al., 2000, Rossetti et al., 2013). However, during the middle to late Miocene, as a consequence of Andean uplift the early transcontinental palaeo-Amazonas hydrographic system started to transport massive amounts of siliciclastic sediments to the equatorial Atlantic coast (Figueiredo et al., 2009; Watss et al., 2009), and together with the sedimentary output of coastal plain drainages brought carbonate production to an end. Riverine input decreased water transparency and changed water chemical parameters (including salinity), which combined with the burial effect of sediment over calcareous fauna triggered the collapse of carbonate production (Aguilera et al., 2014, 2017a). However, the oldest evidence of Andean sediments reaching the Amazon delta, and thus the onset of a transcontinental Amazon river, is 9.4 to 9.0 Ma (Hoorn et al 2017) while we have dated the Atalaia outcrop as 14.2 – 12.7 Ma. This discrepancy is still unsolved. It could be possible that Atalaia is not indeed the top of the Pirabas Formation, or that there is a large unconformity between Pirabas and Barreira formations, and most of the accumulation of the 12-9 Ma interval has been eroded away. An alternative third hypothesis could be proposed, namely, that the collapse of the

carbonate platform in the eastern Amazonia is related to the direct progradation of the siliciclastic Barreiras Formation, which records the last uplift-subsidence event of the Brazilian coast related to the Atlantic Ocean opening (Rossetti et al., 2013), over the carbonate platform, thus having nothing to do with the onset of the Amazon delta.

Several large-scale processes have affected the major reservoirs of Neogene tropical marine biodiversity along the equatorial margin of South America. Thus, reconstructing the entire Pirabas Formation is of paramount importance for understanding the origin and evolution of South American marine ecosystems.

6. Conclusions

(1) Macro and microfossil assemblages suggest a middle Miocene age for the uppermost Pirabas Formation at the Atalaia outcrop. (2) The Atalaia section records in detail the dynamics of a coastal palaeoenvironment dominated by coastal lagoons with mangrove forests under the influence of a tidal regime (mudstones, characterized by the non-preservation of benthic foraminifera and the occurrence of crustaceans, ichnofossils and pyritized leaves and trunks), a shallow inner platform (packstone to floatstones dominated by molluscs, large soritids and calcareous algae); a surf zone affected by wave and current energy (poorly consolidate wackstone, characterized by the accumulation of benthic foraminifera, ostracods and echinoderms). (3) The fossil frameworks and sedimentary palaeoevironments are responsible for the heterogeneity in the porosity values. (4) The ultimate driver of the collapse of Pirabas carbonate production is still uncertaing, but is most likely related to a the transition to a mainly siliclastic depositional environment. (5) The Pirabas Formation could become a facies model for Neogene tropical carbonate deposits of the tropical Atlantic. (6) The use of high technological resources and innovative

solutions together with improved laboratory techniques provides accurate and valuable results even in settings characterized by complex and destructive diagenesis.

Author contributions

OA, ACRN, RL and OOA conceived and designed the experiment. OA, AAEN, ACRN and CWM performed field trip and sample collections. OA, RL, OOA performed the experiment. OA, RL, OOA, AH, AAEN, ACRN, CWM, VTK, MVAM, GC, BBD, SAFS-C, KB and CJ analysed the information context. OA and GC wrote the paper. OA, GC, CJ, BBD, MVAM, ACRN, VTK, RL, SAFS-C and OOA revised and edited the manuscript.

Competing financial interests

The authors declare no competing interest

Acknowledgments

The authors would like to thank the National Mining Agency of Brazil (ANM) for authorization to collect samples at the Pirabas Formation in the Atalaia outcrop (COPAL Protocol number 043/2018 to OA). Many thanks to Stephen Cairns and Félix Rodriguez from the Smithsonian and Kamil Zágoršek from the Brno University of Technology of Czech Republic, for collaboration in the preliminary identification of corals and bryozoans (respectively). The authors are grateful to the participants in the PPGG-UFPA Paleontology postgraduate course 2018 for support this research during field trip and with laboratorial procedures. Thanks to Joelma Lobo (UFPA), Mauro Geraldes and Marcu Helenio (UERJ) by help us with the preparation of petrographic thin sections and SEM image respectively. Many thanks to Ismar Carvalho, Leonardo Borghi and Luis Fernando da Silva from the

Federal University of Rio de Janeiro (UFRJ) by the access to the Laboratory of Sedimentary Geology to use the Petrographic Microscope. Flavia Figueiredo and Rafael da Silva collaborated with the access to the paleontological collections in the UFRJ and CPRM repository, respectively. Many thank to Daniel Lima from the Federal Fluminense University and to Christiano Ng from the CENPES-PETROBRAS for reviews the manuscript. The authors are grateful to Xavier Crosta (Associated Editor of Marine Micropaleontology) and anonymous reviewers for the conments, suggestions and corrections to improve the final manuscript. This study was funded by the Brazilian Council of Science and Technological Development - CNPq (grant 404937/2018-7 and productivity researches 305269/2017-8 to OA), and Coordenação de Aperfeiçoamento de Pessoal de Nível Superior - Brasil (CAPES) (grant PBMAC-UFF, finance code 001 to KB).

References

Abreu W.S., Regali, M.P., Shimabukuro, S., 1986. O Terciário da plataforma continental do Maranhão e Pará, Brasil. Bioestratigrafia e evolução paleoambiental. An 34º Cong Brasileiro Geol. 1, 145-156.

Aguilera, O., Páes, E., 2012. The Pirabas Formation (Early Miocene from Brazil) and the Tropical Western Central Atlantic Subprovince. Bol. Mus. Para. Emílio Goeldi. Ciênc. Nat. 7, 29-45.

Aguilera O.A., Moraes-Santos H., Costa, S., Fumio, O., Jaramillo, C., 2013a. Ariid sea catfishes from the coeval Pirabas (Northeastern Brazil), Cantaure, Castillo (Northwestern Venezuela) and Castilletes (North Colombia) formations (Early Miocene), with description of three new species. Swiss J Palaeontol. doi:10.1007/s13358-013-0052-4

Aguilera, O., Lundberg, J., Birindelli, J., Sabaj, M. Jaramillo, C., Sánchez-Villagra, M., 2013b. Palaeontological evidence for the last temporal occurrence of the ancient western Amazonian River outflow into the Caribbean. PlosOne. doi: 10.1371/journal.pone.0076202

Aguilera, O., Guimaraes, J.T.F., Moraes-Santos, H., 2013c. Neogene Eastern Amazon carbonate platform and the palaeoenvironmental interpretation. Swiss J Palaeontol. doi: 10.1007/s13358-013-0051-5.

Aguilera, O.A., Schwarzhans, W., Moraes-Santos, H., Nepomuceno, A., 2014. Before the flood: Miocene otoliths from eastern Amazon Pirabas Formation reveal a Caribbean-type fish fauna. J S Am Earth Sci. 56, 422-446.

Aguilera, O., Luz, Z., Carrillo-Briceño, J., Kocsis, L., Vennemann, T. W., Toledo, P. M., Nogueira, A., Amorin, K. B., Moraes Santos, H., Polck, M. R., Ruivo, M. L., Linhares, A.P., Monteriro Neto, C., 2017a. Neogene sharks and rays from the Brazilian 'Blue Amazon'. PlosOne. 12(8): e0182740. https://doi.org/10.1371/journal.pone.0182740

Aguilera, O., Silva, G.O.A., Lopes, R.T., Machado, A.S., dos Santos, T.M., Marques, G., Bertucci, T., Aguiar, T., Carrillo-Briceño, J., Rodriguez, F., Jaramillo, C., 2017b. Neogene Proto-Caribbean porcupinefishes (Diodontidae). PlosOne 12(7): e0181670. https://doi.org/10.1371/journal.pone.0181670.

Almeida, F.F.M., Brito Neves, B.B., Carneiro, C.D.R., 2000. The origin and evolution of the South American platform. Earth-Sci Rev. 50, 77-111. https://doi.org/10.1016/S0012-8252(99)00072-0

Allahkarampour, D.M., Vaziri-Moghaddam, H., Seyrafian, A. Behdad, A. (Ghabeishavi)., 2018. Oligo-Miocene carbonate platform evolution in the northern margin of the Asmari

intra-shelf basin, SW Iran. Mar Petrol Geol. 92, 437-461. https://doi.org/10.1016/j.marpetgeo.2017.11.008

Antonioli, L., de Araújo Távora, V., Dino, R., 2015. Palynology of carcinolites and limestones from the Baunilha Grande Ecofacies of the Pirabas Formation (Miocene of Pará State, northeastern Brazil), J S Am Earth Sci. 62, 134-147. doi: https://doi.org/10.1016/j.jsames.2015.05.005

Barbosa, M. M., 1961. *Steginoporella pirabensis* n. sp., Briozoário da Formação Pirabas, Estado do Pará, Brasil. An. Acad. Bras. Ciênc. 31 (1), 109-111.

Beurlen, K., 1958a. Contribuição à paleontología do estado do Pará. Crustáceos decápodes da Formação Pirabas. Bol. Mus. Para. Emílio Goeldi, Nov. Série Geol. 5, 1-48.

Beurlen, K., 1958b. Contribuição à paleontología do estado do Pará. Um Balanomorfo da Formaçai Pirabas. Bol. Mus. Para. Emílio Goeldi, Nov. Série Geol. 6, 1-7.

Berggren, W.A., Kent, D.V., Swisher, C.C., Aubry, M-P., 1995. A revised Cenozoic geochronology and chronostratigraphy. Geochronology Time Scalae and Global Stratigraphic Correlation. SEPM (Society for Sedimentary Geology). Special Publication. 54: 129-212.

Birkenmajer, K., Jednorowska, A., 1997. Early Oligocene foraminifera from Kap Brewster, East Greenland. Ann Sci Geol Poloniae. 67: 155-173.

BouDagher- Fadel, M.K., 2008. Evolution and geological significance of larger benthic Foraminifera. Developments in Palaeontology and Stratigraphy. 21. ELSEVIER, 1- 544.

BouDagher-Fadel, M.K., Price, G.D., 2010. Evolution and paleogeographic distribution of the lepidocyclinids. J Foram Research. 40, 79-108.

BouDagher-Fadel, M.K., Price, G.D., Koutsoukos, E.A.M., 2010. Foraminiferal biostratigraphy and paleoenvironments of the Oligocene-Miocene carbonate succession in Campos Basin, southeastern Brazil. Stratigraphy 7 (4), 283-299.

Borges, K.A., 2016. Paleoambiente, paleogeografia e isótopos de carbono e oxigênio de depósitos carbonáticos miocenos da Plataforma Bragantina, NE do estado do Pará, Brasil. PhD. These. Univ Federal do Pará, Inst Geociên. Brasil.

Braga, J.C., Vescogni, A., Bosellini, F.R., Aguirre, J., 2009. Coralline algae (Corallinales, Rhodophyta) in the western and central Mediterranean Messinian reefs. Palaeogeogra Palaeoclimatol Palaeoeco. 275, 113-128.

Brandano, M., Corda, L., 2002. Nutrients, sea level and tectonics: constrains for the facies architecture of a Miocene carbonate ramp in central Italy. Terra Nova 14, 257-262. https://doi.org/10.1046/j.1365-3121.2000.00419.x

Brandano, M., Rezza, V., Tomasseti, L., Pedley, M., Matteucci, R., 2009. Facies analysis and palaeoenvironmental interpretation of the Late Oligocene Attard Member (Lower Coralline Limestone Formation), Malta. Sedimentology 56, 1138-1158. https://doi.org/10.1111/j.1365-3091.2008.01023.x

Brandão, J.A.S.L., Feijó, F.J., 1994. Bacia do Foz do Amazonas: Bol. Geociên Petrobrás (Rio de Janeiro). 8 (1), 91-100.

Brito, I.M., 1972. Contribuição ao conhecimento dos Crustáceos Decápodos da Formação Pirabas. II – O gênero *Uca* (Brachyura, Ocypodidae). An. Acad. Bras. Ciênc. 44 (1), 95-98.

Buchbinder, B., 1996. Miocene carbonates of the Eastern Mediterranean, the Red Sea and the Mesopotamian Basin: Geodynamic and eustatic controls. In: Franseen, E.K., Esteban,

M., Ward, W.C., Rouchy, J-M. (eds). Models for carbonate stratigraphy from Miocene reef complexes of Mediterranean regions.. https://doi.org/10.2110/csp.96.01.0089

Coletti, G., El Kateb, A., Basso, D., Cavallo, A., Spezzaferri, S., 2017. Nutrient influence on fossil carbonate factories: evidence from SEDEX extractions on Burdigalian limestones (Miocene, NW Italy and S France). Palaeogeogr Paleoeoclimatol Paleoecol. 475, 80-92. http://dx.doi.org/10.1016/j.palaeo.2017.03.005

Coletti, G., Basso, D., Corselli, C., 2018. Coralline algae as depth indicators in the Sommières Basin (early Miocene, Southern France). Geobios 51, 15-30. https://doi.org/10.1016/j.geobios.2017.12.002

Coletti, G., Basso, D., Betzler, C., Robertson, A.H.F., Bassio, G., El Kateb, A., Foubert, A., Meilijson, A., Spezzaferri, S., 2019. Environmental evolution and geological significance of the Miocene carbonates of the Eratosthenes Seamount (ODP Leg 160). Palaeogeogra Palaeoclimatol Palaeoeco. 530, 217-235.

Culver, S.J., 1988. New foraminiferal depth zonation of the Northwestern Gulf of Mexico. Palaios 3 (1), 69-85. doi: 10.2307/3514545

Damuth, J.E., Kumar, N., 1975. Amazon Cone: morphology, sediments, age, and grown pattern. Geol Soc Am Bull. 86, 863-878.

De Araújo, O.M.O., Sharma, K.V., Machado, A.S., Santos, T.M.P., Ferreira, C.G., Straka, R., Lopes, R.T., 2018. Representative elementary volume in limestone sample. J Instrument. 13(10), C10003.

Dill, M.A., Vaziri-Moghaddam, H., Seyrafian, A., Behdad (Ghabeishavi), A., 2018. Oligo-Miocene carbonate platform evolution in the northern margin of the Asmari intra-shelf basin, SW Iran. Mar Petroleum Geol. 92. https://doi.org/10.1016/j.marpetgeo.2017.11.008

Duarte, L., 2004. Paleoflórula. In: Rossetti, D., Goes, A. (eds.). O Neogeno da Amazônia Oriental. Belém: Museu Paraense Emilio Goeldi. p. 13-52.

Dunham, R. J., 1962. Classification of carbonate rocks according to depositional texture. In: Ham, W. E. (ed.). Classification of carbonate rocks: Am Assoc Petrol Geologists Mem., p. 108-121.

Egger, L.M., Bahr, A., Friedrich, O., Wilson, P.A., Norris, R.D., van Peer, T.E., Lippert, P.C., Liebrand, D., Pross, J., 2018. Sea-level and surface-water change in the western North Atlantic across the Oligocene-Miocene Transition: A palynological perspective from IODP Site U1406 (Newfoundland margin). Mar Micropaleontol. 139, 57-71. https://doi.org/10.1016/j.marmicro.2017.11.003.

Ehrenberg, S.N., Eberli, G.P., Baechle, G., 2006. Porosity–permeability relationships in Miocene carbonate platforms and slopes seaward of the Great Barrier Reef, Australia (ODP Leg 194, Marion Plateau). Sedimentology 53, 1289-1318. doi: 10.1111/j.1365-3091.2006.00817.

Fernandes, J. M. G., 1984. Paleoecology of Pirabas Formation, Pará state. In: 33º Brazilian Cong Geol. 33, An. Acad. Bras. Ciênc. SBG. 1, 330-340.

Fernandes, J.M.G., 1988. Biostratigraphy of Pirabas Formation, Pará state. In: Brazilian Cong Geol 35, An. Acad. Bras. Ciênc. SBG. 1, 2376-2382.

Fernandes, M.J.G., Távora, V.A., 1990. Estudo dos Foraminíferos da Formação Pirabas procedentes do furo CB- UFPa-P1 (85), município de Capanema, Estado do Pará. An 26° Cong Brasilerio Geol. 1, 470-475.

Ferreira, C.D., 1964. Contribuição à paleontologia do estado do Pará. Um novo *Xancus* da Formação Pirabas, VII (Mollusca-Gastropoda). Bol. Mus. Para. Emílio Goeldi, Nov. Série Geol. 10, 1-14.

Fernandes, A.C.S., 1979. Contribuição à paleontologia do estado do Pará. Scleractinia da Formação Pirabas (Mioceno inferior) e suas implicações paleoecológicas (Coelenterata, Antohozoa). Bol. Mus. Para. Emílio Goeldi, Nov. Série Geol. 22: 1-39.

Fernandes, A.C.S., 1981. Contribuição à paleontologia do estado do Pará. Um novo *Flabellum* (Anthozoa, Scleractinia). Bol. Mus. Para. Emílio Goeldi, Nov. Série Geol. 24: 1-8.

Ferreira, C.S., Macedo, A.C.M., Assis, J.F.P., 1978. A Formação Pirabas no estado do Pará – novo registro de subsuperfície: Belém (furo 4BE-01-PA, CPRM). An. Acad. Bras. Ciênc. 50(3), 427.

Ferreira, C.S., Francisco B.H.R., 1988. As relações da Formação Pirabas (Oligoceno-Mioceno), com as formações continentais terciárias no NE do Pará. 35° Cong Brasileiro Geol. 2, 761-764.

Ferreira-Penna, D.S., 1876. Breves notícias sobre os sambaquís do Pará. Arq Museu Nacional. 1, 85-89.

Figueiredo, J., Zalán, P.V., Soares, E.F., 2007. Bacia da Foz do Amazonas. Bol. Geociên. PETROBRAS 15 (2) 299-309.

Figueiredo, J., Hoorn, C., Van der Ven P., Soares, E., 2009. Late Miocene onset of the Amazon River and the Amazon deep-sea fan: evidence from the Foz do Amazonas Basin. Geology 37, 19-622. doi:10.1130/ G25207A.1

Fiorini, F., Jaramillo, C.A. 2007. Paleoenvironmental reconstruction of the Oligocene-Miocene deposits of Southern Caribbean (Carmen de Bolivar, Colombia) based on benthic foraminifera. Bol Geol. 29 (2), 47-55.

Flügel, E., 2010. Microfacies of Carbonate Rocks: Analysis Interpretation and Application. Springer, New York.

Francisco, B.H.R., Loewenstein, P., Silva, O.F., Silva, G.G., 1971. Contribuição a Geologia da Folha de São Luís (SA-23) no Estado do Pará. III- Estratigrafia. IV-Recursos Minerais. Bol. do Mus. Para. Emílio Goeldi, Nov Sér Geol. 17, 1-40.

Freimann, B.C., Alves, J.G.V., Silva, M.W.C., 2014. Estudo hidrogeológico através de perfis geofísicos de poços - Salinópolis-PA. Águas subterrâneas 28 (1), 14-30.

Góes, A.M., Rossetti, D. Nogueira, A., Toledo, P.M., 1990. Modelo deposicional preliminar da Formação Pirabas no Nordeste do Estado do Pará. Bol. Mus. Para. Emílio Goeldi. Ciênc. Terra 2, 3-15.

Goldner, A., Herold, H., Huber, M., 2014. The challenge of simulating the warmth of the mid-Miocene climatic optimum in CESM1. Climate Past 10: 523-536. doi:10.5194/cp-10-523-2014.

Gonzalez, R.C., Woods, R.E . 2002. Digital Image Processing (2nd.Ed.). Prentice Hall, USA. Companion Website: www.premhall.com/gozalezwoods

Grabau A.W., 1904. Classification of sedimentary rocks. Am Geol. 33: 228-247.

Hayward, B.W., 2014. "Monospecific"and near-monospecific benthic foraminiferal faunas, New Zealand J Foram Research 44 (3), 300-315. doi: 10.2113/gsjfr.44.3.300

Haq, B.U., Hardenbol, J., Vail, P.R., 1987. Chronology of fluctuating sea levels since the Triassic. Science 235, 1156-1167. https://doi.org/10.1126/science.235.4793.1156.

Hebert, V., Garing, L. Luquot, Pezard, P.A., Gouze, P., 2014. Multi-scale X-ray tomography analysis of carbonate porosity. In: Agar, S.M., Geiger, S. (eds) Fundamental Controls on Fluid Flow in Carbonates. Geological Society, London, Special Publications, 406. http://dx.doi.org/10.1144/SP406.12

Hoorn, C., Bogotá-A., G., Romero-Baez, M., Lammertsma, E. I., Flantua, S. G. A., Dantas, E. I., Dino, R., do Carmo, D. A., Chemale jr., F., 2017. The Amazon at Sea: Onset and

stages of the Amazon River from a Neogene record at the Brazil Equatorial Margin: Onset and stages of the Amazon River from a marine record, with special reference to Neogene plant turnover in the drainage basin. Glo Planet Change. dx.doi.org/10.1016/j.gloplacha.2017.02.005

Janjuhah, H.T., Vintaned, J.A.G., Salim, A.M.A., Faye, I., Shah, M.M., Ghosh, D.P., 2017a. Microfacies and depositional environments of Miocene isolate carbonate platforms from Central Luconia, offshore Sarawak, Malaysia. Acta Geol Sin. 91 (5), 1778-1796. https://doi.org/10.1111/1755-6724.13411

Janjuhah, H.T., Salim, A.M.A., Ghosh, D.P., Wahid A., 2017b. Diagenetic process and their effect on reservoir quality in Miocene carbonate reservoir, offshore, Sarawak, Malaysia In: Icipeg 2016, Springer, p. 545-558.

Jaramillo, C., Rueda, M., Torres, V., 2011. A palynological zonation for the Cenozoic of the Llanos and Llanos foothills of Colombia. Palynology 35, 46-84. http://dx.doi.org/10.1080/01916122.2010.515069.

John, C.M., Mutti, M., Adatte, T., 2003. Mixed carbonate-siliciclastic recordo n the North Africa margin (Malta) - coupling of weathering processes and mid Miocene climate. GSA Bulletin 2, 217-229. https://doi.org/10.1130/00167606(2003)115<0217:MCSROT>2.0.CO;2

Johnson, K.G., Sanchez-Villagra, M.R., Aguilera, O., 2009. The Oligocene-Miocene transition on coral reefs in the Falcón Basin (NW Venezuela). Palaios 24, 59-69. doi: 10.2110/palo.2008.p08-004r

Kominz, M.A., Browning, J .V., Miller, K.G., Sugarman, P.J., Mizintseva, S., Scotese, C.R., 2008. Late Cretaceous to Miocene sea-level estimates from the New Jersey and

Delaware coastal plain coreholes: an error analysis. Basin Res. 20, 211-226. https://doi.org/10.1111/j.1365-2117.2008.00354.x

Kroh, A., Nebelsick, J.H., 2010. Echinoderms and Oligo-Miocene carbonate systems: potential applications in sedimentology and environmental reconstruction. Int. Assoc. Sedimentol. Spec. Publ. 42: 201-228. https://doi.org/10.1002/9781118398364.ch12

Langer, M.R., 2008. Foraminifera from the Mediterranean and the Red Sea. Por, F.D.(ed). The Improbable Gulf: Environment, Biodiversity, and Preservation. Magnes Press, 399-417.

Langer, M.R., Hottinger, L., 2000. Biogeography of selected "larger" foraminifera. Micropaleontology 46 (1), 105-126.

Laut, L.L.M., Ferreira, D.E.S., Santos, V.F., Figueiredo Jr., A.G., Carvalho, M.A., Machado, O.F., 2010. Foraminifera, thecamoebians and playnomorphs as hydrodynamic indicators in Araguari estuary, Amazonian coast, Amapá state – Brazil. An Inst Geociên UFRJ. 33(2), 52-65.

Leckie, R.M., Olson, H.C., 2003. Foraminifera as proxies for sea-level change on siliciclastic margins. In: Olson, H.C., Leckie, R.M. (eds). Micropaleontological proxies for sea-level change and stratigraphic discontinuities, SEPM Spec. Publ. 75, 5-19.

Leigh, E.G., O'Dea, A., Vermeij, G.J., 2013. Historical biogeography of the Isthmus of Panama. Biol Rev. doi: 10.1111/brv.12048

Leite, F.P.R., 1997. Palinofloras Neógenas da Formaçao Pirabas e Grupo Barreiras, área litorânea nordeste do estado do Pará, Brasil. MSc. These, Inst Geociên Univer São Paulo, Brasil.

Leite, F.P.R., 2004. Palinologia. In: Rossetti, D.F., Góes, A.M. (eds). O Neógeno da Amazonia Oriental. Belém: Mus Paraense Emílio Goeldi, p. 55-90.

Lokier S.W., Wilson M.E.J., Burton L.M., 2009. Marine biota response to clastic sediment influx: A quantitative approach. Palaeogeogr. Palaeoclimatol. Palaeoecol. 281: 25-42.

Longhitano, S.G., Mellere, D., Steel, R.J., Ainsworth, R.B., 2012. Tidal depositional systems in the rock record: A review and new insights. Sed Geol. 279, 2-22. https://doi.org/10.1016/j.sedgeo.2012.03.024

Luque, J., Schweitzer, C.E., Santana, W., Portell, R.W., Vega, F.J., Klompmaker, A.A., 2017. Checklist of fossil decapod crustaceans from tropical America. Part I: Anomura and Brachyura. Nauplius 25: e2017025. doi: 10.1590/2358-2936e2017025

Ma, Z.L., Li, Q.Y., Liu, X.Y., Luo, W., Zhang, D.J., Zhu, Y.H. 2017. Palaeoenvironmental significance of Miocene larger benthic foraminifera from the Xisha Islands, South China Sea. Palaeoworld 27, 145-157. doi: 10.1016/j.palwor.2017.05.007

Martínez, S., Ramos, M.I.F., McArthur, J.M., Rio, C.J., Thirlwall, M.F., 2017. Late Burdigalian (Miocene) age for pectinids (Mollusca-Bivalvia) from the Pirabas Formation (northern Brazil) derived from Sr-isotope (87Sr/86Sr) data. N. Jb. Geol. Palont. Abh. 284 (1), 57-64. doi: 10.1227/njgpa/2017/0650

Mateu-Vicens, G., Hallock, P., Brandano, M., 2009. Test-shape variability of *Amphistegina* D'Orbigny, 1826 As a Paleobathymetric Proxy: Application to two Miocene examples. Geologic problem solving with Microfossils: A volume in Honor of Garry D. Jones. SEPM (Society for Sedimentary Geology) Spec Public. 93: 67-82.

Maury, C.J., 1925. Fósseis terciários do Brasil com descrição de novas formas Cretáceas. Serviço Geológico e Mineralógico do Brasil, Monografia 4, 665 p.

Mihaljevic, M., Renema, W., Welsh, K., Pandonlfi, J.M., 2014. Eocene–Miocene shallow-water carbonate platforms and increased hábitat diversity in Sarawak, Malaysia. Palaios 29: 378-391. http://dx.doi.org/10.2110/palo.2013.129

Mooi, R., Martínez, S.A., Del Río, C.J., Ramos, M.I.F., 2018. Late Oligocene-Miocene non-lunulate sand dollars of South America: Revision of abertellid taxa and descriptions of two new families, two new genera, and a new species. Zootaxa 4369 (3), 301-326. doi.org/10.11646/zootaxa.4369.3.1

Muricy, G., Domingos, C., Távora, V.A., Ramalho, L.V., Pisera, A., Taylor, P., 2016. Hexactinellid sponges reported from shallow waters in the Oligo-Miocene Pirabas Formation (N Brazil) are in fact cheilostome bryozoans, J S Am. Earth Sci. doi: 10.1016/j.jsames.2016.10.003

Murray, J.W., 2006. Ecology and applications of benthic foraminifera. Cambrige University Press, Cambridge.

Ma, Z.L., Li, Q.Y., Liu, X.Y., Luo, W., Zhang, P.J., Zhu, Y.H., 2017. Palaeoenvironmental significance of Miocene larger benthic foraminifera from the Xisha Islands, South China Sea. Palaeoworld 27, 145-157. doi: 10.1016/j.palwor.2017.05.007

Nogueira, A.A.E., Nogueira, A.C.R., 2017. Ostracod biostratigraphy of the Oligocene-Miocene carbonate platform in the Northeastern Amazonia coast and its correlation with the Caribbean Region. J S Am Earth Sci. 80, 389-403.

Pamplona, H.R.P., 1969. Litoestratigrafia da Bacia Cretácea de Barreirinhas. Rio de Janeiro. Bol. Téc. PETROBRAS 12 (3), 261-290

Paula-Couto, C., 1967. Contribuição à paleontologia do estado de Pará. Um sirênio na Formação Pirabas. 1º Simpósio sobre a Biota Amazônica. Atas, CNPq 1, 345-357.

Petri, S., 1954. Foraminíferos fósseis da Bacia do Marajó. Boletim da Faculdade de Filosofia, Ciên Letras Univ São Paulo. Geologia. 11: 4-144.

Petri, S., 1957. Foraminíferos Miocênicos da Formação Pirabas. Boletim da Faculdade de Filosofia, Ciên Letras Univ São Paulo. Geologia. 216, 1-172.

Ramalho, L.V., Távora, V.A., Tilbrook, K.J., Zágorsek, K., 2015. New species of *Hippopleurifera* (Bryozoa, Cheilostomata) from the Miocene Pirabas Formation, Pará state, Brazil. Zootaxa 3999(1), 125-134. http://dx.doi.org/10.11646/zootaxa.3999.1.8

Ramalho, L.V., Távora, V.A., Zagorsek, K., 2017. New records of the bryozoan *Metrarabdotos* from the Pirabas Formation (Lower Miocene), Pará State, Brazil Palaeontol Electron. 20.2.32A, 1-11. https://doi.org/10.26879/704

Rashid, F., Glover, P.W.J., Lorinczi, P., Collier, R., Lawrence, J., 2015. Porosity and permeability of tight carbonate reservoir rocks in the north of Iraq. J Petrol Sci Eng.133, 147-161. https://doi.org/10.1016/j.petrol.2015.05.009

Reid, C.M. 1998. Stratigraphy, paleontology, and tectonics of lower Miocene rocks in the Waipatiki/Mangatuna area, southern Hawke's Bay, New Zealand. New Zealand J Geol Geophy. 41, 115-131. doi: 10.1080/00288306.1998.9514796

Roozpeykar, A., Maghfouri-Moghaddam, I., Yazdi, M., Yousefi-Yegane, B., 2019. Facies and paleoenvironmental reconstruction of Early-Middle Miocene deposits in the north-west of the Zagros Basin, Iran. Geol Carpathica. 70(1), 75-87. doi: 10.2478/geoca-2019-0005

Rossetti, D., 2001. Late Cenozoic sedimentary evolution in northeastern Pará, Brazil, within the context of sea level changes. J S Am Earth Sci. 14, 77-89. https://doi.org/10.1016/S0895-9811(01)00008-6

Rossetti, D., Góes, A., 2004. Geologia. In: Rossetti, D., Goes, A. (eds). O Neogeno da Amazônia Oriental. Belém: Mus Paraense Emilio Goeldi. p. 13-52

Rossetti, D.F., Bezerra, F.H.R., Dominguez, J.M.L., 2013. Late Oligocene–Miocene transgressions along the equatorial and eastern margins of Brazil. Earth Sci Rev. 123, 87-112. https://doi.org/10.1016/j.earscirev.2013.04.005

Roozpeykar, A, Moghaddam, I,M., 2016. Benthic foraminifera as biostratigraphical and paleoecological indicators: An example from Oligo-Miocene deposits in the SW of Zagros basin, Iran. Geosci Front. 7, 125-140. http://dx.doi.org/10.1016/j.gsf.2015.03.005.

Sadeq, Q.M., Wan Yusoff, W.I.B., 2015. Porosity and permeability analysis from well logs and core in fracture, vugy and intercrystalline carbonate reservoirs. J Aquac Res Dev. 6, 371. doi: 10.4172/2155-9546.1000371.

Santiago, F., Ricardi-Branco, F., 2018. Interpretações paleoclimáticas a partir da tafoflora de Caieira, Formação Pirabas, Oligoceno/Mioceno da Amazônia Oriental, Pará, Brasil. Rev Bras Paleontol. 22 (3), 265-271.

Santos, M.E.C.M., 1958. Equinóides miocênicos da Formação Pirabas. Bol Div Geol Mineral. 179, 1-24.

Santos, M.E.C.M., 1967. Equinóides miocênicos da Formação Pirabas. 1º Simp Biota Amazônica. Atas CNPq. 1, 407-410.

Santos, R.S., Travassos, S., 1960. Contribuição a paleontologia do estado do Pará. Peixes fósseis da Formação Pirabas. Monog Div Geol Mineral. 16, 1-35.

Sarkar, S., Ghosh, A.K., Ghosh, A.K., Rao, G.M.N., 2016. Coralline algae and benthic foraminifera from the Long Formation (middle Miocene) of the little Andaman Island, India: Biofacies Analysis, Systematics and Palaeoenvironmental Implications. J Geol Soc India. 87, 69-84. https://doi.org/10.1007/s12594-016-0375-z

Schaller, H., Vasconcelos, D. N., Castro, C. C., 1971. Estratigrafia preliminar da bacia sedimentar da Foz do Amazonas. In: An 25 Cong Brasileiro Geol. São Paulo. SBG. 3, 189-202.

Schejter, L., Bremec, C., 2015. First record and range extension of the Antarctic coral *Flabellum* (*Flabellum*) *impensum* Squires, 1962 (Cnidaria: Scleractinia) in Argentinean coastal waters. Mar Biodivers Rec. 8, 1-3. doi:10.1017/S1755267215000858.

Schmoker, J.W., Halley, R.B., 1982. Carbonate porosity versus depth: A predictable relation for South Florida: AAPG Bulletin 66, 2561-2570.

Silva, S.R.P., Maciel, R.R., Severino, M.C.G., 1998. Cenozoic tectonics of Amazon mouth basin. Geo-Mar Lett. 18, 256-262. https://doi.org/10.1007/s003670050077

Silva, C.B.S., 2016. Palinologia da Formação Pirabas, nos municípios de Primavera e Salinópolis, nordeste do estado do Pará, Brasil. MSc Thesis. Univ Federal do Pará (UFPA), Brasil.

Soares, E.F., Zalán, P.V., Figueiredo, J-J.P., Trosdtorf Jr., I., 2007. Bacia do Pará. Maranhão. Bol. Geociên PETROBRAS 15 (2), 321-329.

Soares Jr., A.V., Hasui Y., Costa J.B.S., Machado F.B., 2011. Evolução do rifteamento e paleogeografia da margem Atlântica Equatorial do Brasil: Triássico ao Holoceno. Geociências-UNESP 30 (4), 665-692.

Sousa, S.H.M., Fairchild, T.R., Tibana, P., 2003. Cenozoic biostratigraphy of larger foraminifera from the Foz do Amazonas Basin, Brazil. Micropaleontology 49 (3), 253-266.

Stewart, J.A., James, R.H., Anand, P., Wilson, P.A., 2017. Silicate weathering and carbon cycle controls on the Oligocene-Miocene transition glaciation. Paleoceanography 32, 1070-1085. doi: https://doi.org/10.1002/2017PA003115

Távora, V., Fernandes, J.M., 1999. Estúdio de los foraminíferos de la Formación Pirabas (Mioceno Inferior), estado de Pará, Brasil y su correlación con faunas del Caribe. Rev Geol Am Central. 22, 63-74.

Távora, V., Dos Santos, A.A.R., Araújo, R.N., 2010. Localidades fossilíferas da Formação Pirabas (Mioceno inferior). Bol Mus Para Emílio Goeldi. Ciênc Nat. 5 (2), 207-224.

Távora, V., Souza, B.L.P, Neto, I.L.A.N., 2014. Micropaleontologia da litofácies recifal da Formação Pirabas (Mioceno inferior), Estado do Pará, Brasil. An Inst Geociên-UFRJ. 37 (2), 100-110.

Trosdtorf Jr., I., Zalán, P.V., Figueiredo, J-J.P., Soares, E.F., 2007. Bacia de Barreirinhas. Bol. Geoc. PETROBRAS 15 (2), 331-339.

Zágoršek K, Ramalho LV, Berning B, Távora V.A., 2014. A new genus of the family Jaculinidae (Cheilostomata, Bryozoa) from the Miocene of the tropical western Atlantic. Zootaxa 3838 (1), 98-112. http://dx.doi.org/10.11646/zootaxa.3838.1.5

Vahrenkamp V.C., 1998. Miocene carbonates of the Loconia province, offshore Sarawak: implications for regional geology and reservoir properties from Strontium-isotope stratigraphy. Bull Geol Soc Malalysia. 42, 1-13.

Vasconcellos, R.V.A., 2013. 11º Round Foz de Amazonas Basin, Brasil. Agencia Nacional do Petróleo (ANP). On line access Nov.10.2019: http://rodadas.anp.gov.br/arquivos/Round11/Seminarios_r11/tec_ambiental/Bacia_da_Foz_do_Amazonas.pdf

Wade, B.S., Pearson, P.N., Berggren, W.A., Pälike, H., 2011. Review and revision of Cenozoic tropical planktonic foraminiferal biostratigraphy and calibration to the geomagnetic polarity and astronomical time scale. Earth Sc Reviews. 104, 111-142.

Watts, A.B., Rodger, M., Peirce, C., Greenroyd, C.J., Hobbs, R.W., 2009. Seismic structure, gravity anomalies, and flexure of the Amazon continental margin, NE Brazil. J Geophys Res. 114, B07103, doi:10.1029/2008JB006259

White, C.A., 1887. Contribuição à Paleontologia do Brasil. Arq Mus Nacional. 7, 1-273.

Wilson M.E.J., Vecsei A., 2005. The apparent paradox of abundant foramol facies in low latitudes: their environmental significance and effect on platform development. Earth-Sc Reviews, 69, 133-168.

Wilson, B., Vincent, H., 2014. Benthonic foraminífera in the Upper Miocene Cruse Formation at Quinam Bay, Trinidad, western tropical Atlantic Ocean, and their palaeoenvironmental significance. Geol Magazine. 151(3), 550-558. doi: 10.1017/S0016756813000496

Wolff, B., Carozzi, A.V., 1984, Microfacies, depositional environments, and diagenesis of the Amapá carbonates (Paleocene–middle Miocene), Foz do Amazonas Basin, offshore NE Brasil: PETROBRAS, Sér Ciênc-Téc-Petról: Seção Expl Petról. 13, 102.

Woodroffe, S.A., Horton, B.P., Larcombre, P., Whitaker, J.E., 2005. Intertidal mangrove foraminífera from the central Great Barrier Reef shelf, Australia: implications for sea-level reconstruction. J Foram Research. 35(3): 259-270.

You, Y., Huber, M., Muller, R. D., Poulsen, C. J., Ribbe J., 2009. Simulation of the Middle Miocene Climate Optimum, Geophys Res Lett. 36, L04702, doi:10.1029/2008GL036571.

Zampetto, V., Schlager, W., Konijnenburg, J-H, Everts A-J., 2003. Depositional history and origin of porosity in a Miocene carbonate platform of Central Luconia, offshore Sarawak. Bull Geol Soc Malalysia. 47, 139-152.

Zoeram, F.Z., Vahidinia, M., Sadeghi, A., Mahboubi, A., Bakhtiar, H.A., 2015. Larger benthic foraminifera: a tool for biostratigraphy, facies analysis and paleoenvironmental interpretations of the Oligo-Miocene carbonates, NW Central Zagros Basin, Iran. Arabian J Geoscien. 8, 931-949. doi: 10.1007/s12517-013-1153-5

Figure and legend

Fig. 1. Location map and the stratigraphic section of the Pirabas Formation (middle Miocene) at the Atalaia outcrop, Brazil (modified from Aguilera et al. 2017a). The petrographic nomenclature follows Grabau (1904) and Dunham (1962). Note the environmental changes from the inner shelf, surf zone and coastal lagoons with mangroves could be controlled by local or regional effects of sea-level fluctuations, sedimentary dynamics linked with the tidal regime and carbonate production. The influx of fine-grained sedimentary mudstones and argillite inhibited the development of large-scale coral-reefs and formed a heterogeneous seafloor consisting of consolidated carbonate substrates with abundant fossil assemblages and soft shale sediment.

Fig. 2. Outcrop of the Pirabas Formation (middle Miocene) at the Atalaia beach (0º 35' 37" S, 47º 18' 54.4" W), Pará State, exposed during the lowest tidal range (0.0); 2, 3, outcrop (base) cutting slices, sample LP&MG-PirAtaS001; 4, 5, outcrop (base) cutting slices, sample LP&MG-PirAtaS002 (note the complexity of fossil remains, empty space, vugs and infilled moulds in the carbonate matrix); 6, outcrop (top) cutting slices, samples LP&MG-PirAtaS001 to 008.

Fig. 3. Example of a large micro CT view of the outcrop (base) cutting slices, sample LP&MG-PirAtaS003 showing details of gastropod moulds of Fusinininae (Fasciolariidae) in the rock matrix and the micro CT volumetric 3D reconstruction.

Fig. 4. Example of a nano CT sequences view (1-4) of outcrop (base) plug sample from LP&MG-PirAtaS003 slice from the Atalaia outcrop showing selected area for volumetric reconstructions of 1, bryozoan *Metrarabdotos* (Metrarabdotosidae); 2, coralline red algae (sterile form of Corallinacea); 3, foraminifera *Spiroloculina* and *Quinqueloculina* (Hauerinidae); *4*, *Echitricolprites* (Bombacaceae) and mollusc bivalve *Lamelliconcha* (Veneridae).

Fig. 5. 3D reconstructions of fossil specimens from the Pirabas carbonate rock at the outcrop (base). 1, dorsal and lateral views of cf. *Orthaulax* (Strombidae); 2, details of ichnofossil *Entobia* cf. *geometrica* fixed to cf. *Orthaulax* shell; 3, juvenile of Olividae (Olivellinae), cf. *Olivella*; 4, shell with a bulbous larval protoconch of a juvenile Fusininae (Fasciolariidae), cf. *Fusinus*; 5, cf. *Fusinus* without protoconch; 6, cf. Ranellidae; 7, Strombidae; 8, large foraminifera next to Strombidae shell; 9, juvenile of cf. Cypraeidae; 10, cf. Naticidae; 11, cf. Arcillaridae; 12, a fragment of cf. Ranellidae; 13, *Conus paraensis* (note the predatory borehole in the shell attacked by boring organisms); 14, Strombidae; 15, Melongenidae; 16, *Arcilla* sp. (Arcillaridae). Sample LP&MG-PirAtaS003.

Fig. 6. 3D reconstructions of fossil specimens from the Pirabas carbonate rock at the outcrop (continued). 1, Dallocardia (Cardiidae); 2, Tellinidae; 3, cf. *Lamelliconcha* (Veneridae); 4, small Tellinidae; 5, *Dallocardia* sp. (Cardiidae); 6, *Cupuladria* sp. (Cupuladriidae); 7, articulate valves of Limidae (note the predatory borehole in the shell attacked by boring organisms); 8, fragments of bryozoan colony of *Pirabasoporella* (Jaculinidae) infilled the shells; 9, Cardidae (note the predatory borehole in the shell); 10,

Trigonocardia?; 11, *Turritella* sp. (Turritellidae); 12, *Trigonocardia*; 13, foraminifera (inside the shell); 14, *Cupuladria* sp. (Cupuladriidae);15, *Metrarabdotos* sp. (Metrarabdotosidae); 16, *Flabellus* sp. (Flabellidae) in anterior, lateral and posterior views; 17, cf. *Flabellus*; 18, a proximal fragment of echinoid spine (cf. *Prionocidaris*) and teste fragment. Sample LP&MG-PirAtaS003.

Fig. 7. 3D reconstructions of fossil specimens from the Pirabas carbonate rock at the outcrop (continued). 1, *Ammodiscus* cf. *peruvianus* Berry, 1928 (Ammodiscidae), dorsal and lateral views; 2, 3, coralline algae (sterile); 4, 5, *Spiroloculina angulata* Cushman, 1917 (Hauerinidae) in rotated views; 6, 7, *Spiroloculina cymbium* d'Orbigny, 1839 (Hauerinidae) in rotated views; 8, 9, *Quinqueloculina crassicarinata* Collins, 1958 (Hauerinidae) in rotated views; 10, *Spirosigmoilinella compressa* Matsunaga, 1955 (Milamminidae); 11, *Pyrgo subsphaerica* (d´Orbigny, 1839) in rotated views. Sample LP&MG-PirAtaS003.

Fig. 8. Photomicrographs of microfossils from Pirabas outcrop (base). 1, *Amphistegina* (Amphisteginidae): amp, and *Planorbulinella* sp.: pla.; 2, 3, *Amphistegina* (Amphisteginidae): amp; 4, echinoid fragment: ech; 5, dissolved fragment of soritids (Soritoidea): sor; 6, indeterminate foraminifera: for; 7, *Globigerina* (Globigerinidae): glo; 8, indeterminate (badly preserved bioclast): ind; 9, *Amphistegina* (Amphisteginidae): amp; 10, regular echinoid spine: ech; 11, sterile coralline algae: alg; 12, indeterminate: ind; 13, *Bigenerina* (Textulariidae): big; 14, 15, mollusc fragment: mol. Sample LP&MG-PirAtaS001.

Fig. 9. Photomicrographs of microfossils from the Pirabas outcrop (base) (continued). 1, Bryozoan: bry; 2, small echinoid spine: ech; 3, *Amphistegina* (Amphisteginidae): amp, and echinoid spine: ech; 4, small coral Flabellidae: fla; 5, *Bigenerina*: big; 6, *Amphistegina* (Amphisteginidae): amp; 7, Cupuladriidae (ventral view of fragment): cup; 8, algae: alg, and ostracods: ost; 9, Bryozoan: bry, and indeterminate foraminifera: for; 10, Soritoidea: sor; 11, miliolids: mil, and *Crototricolpites* (Tricolpatae): cro; 12, echinoid spine: ech; 13, large spine of a regular echinoid: ech; 14, crustacean fragment: cru; 15, spicule of sponge: spo. Sample LP&MG-PirAtaS001.

Fig. 10. Photomicrographs of microfossils from the Pirabas outcrop (base) (continued). 1, echinoid: ech; 2, echinoid fragment: ech; 3, indeterminate: ind; 4, mollusc fragment: mol; 5, Coralline algae: alg; 6, indeterminate rotaliid: rot; 7, Corallinales or Hapalidiales (Corallinaceae): cor; 8, ostracod: ost, and coralline algal nodule (possibly composed of Corallinales and Hapalidiales (Corallinaceae): alg; 9, piritaized *Globigerina* or bulbous air: ind; 10, mollusc fragment: mol; 11, algae ind: alg, and crinoid: cri; 12, foraminifera: for, algae: alg, and probably large miliolids (cf. *Dendritina*): mil; 13, fish vertebrae: fis; 14, foraminifera (mold): for; 15, indeterminate bioclast: bio. Sample LP&MG-PirAtaS001.

Fig. 11. 3D reconstructions of fossil specimens from the Pirabas carbonate rock at the outcrop (top). 1, coralline algae; 2, 3, ind. foraminifera in rotated views; 4, *Flavelus* (Flavelidae) in lateral, anterior and posterior views; 5, *Cupuladria* sp. (Cupuladriidae) in lateral dorsal and ventral views; 6, ind. gastropod in rotated views; 7, *Turritella* (Turretellidae) in rotated views; 8, *Conus* (Conidae) in rotated views; 9, *Strombus*

(Strombidae) in rotated views; 10, *Semele* (Semelidae) in rotated views; 11, *Cupuladria* sp. (Cupuladriidae); 12, shark teeth. Sample LP&MG-PirAtaS004.

Fig. 12. Photomicrographs of microfossils from the Pirabas outcrop (top). 1, Bryozoan: bry, and foraminifera *Amphistegina* (Amphisteginidae): amp; 2, 3, Foraminifera *Pyrgo* sp.: pyr; 4, Bryozoan: bry, and foraminifera ind.: for; 5, echinoid spine; 6, echinoid fragments: ech; 7, *Rotaliida* Delage and Hérouard, 1896: rot; 8, indetermitad: ind; 9, *Globigerina* (Globirenigidae): glo; 10, 11, soritids: sor; 12, foraminifera *Textularia gramen* (d'Orbigny, 1839): tex, micro gasteropod: mol, coralline algae: alg; 13, foraminifera: for, coralline algae: alg, ostracod: ost; 14, algae: alg. Sample LP&MG-PirAtaS004.

Fig. 13. Photomicrographs of microfossils from the Pirabas outcrop (top) (continued). 1, *Pyrgo* sp.: pyr; 2, 3, green algae: alg; 4, bryozoan: bry, indeterminate: ind; 5, algae: alg; 6, *Amphistegina* (Amphisteginidae): amp, bryozoan: bry, indeterminate: ind; 7, large benthic foraminifera ind: for; 8, foraminifera *Nodosarella* sp.: nod; 9, soritid: sor. Sample LP&MG-PirAtaS004.

Fig. 14. Some sporomorphs of Pirabas Formation in Atalaia outcrop. 1, *Crassoretitriletes vanraadshooveni* Germerraad et al. 1968; Maximum diameter 82 µ (slide: 1459; Coord. EF: U35 2; 2, *Deltoidospora adriennis* (Potonié and Gelletich 1933) Fredericksen 1983 Maximum diameter 42 µ (slide: 1459; Coord. EF: Q43 4; 3, *Zonocostites ramonae* Germeraad et al., 1968. Maximum diameter 15 µ, polar view. 4, *Z. ramonae*. Maximum diameter 18 µ, equatorial view. (slide: 1461; Coord EF: P44 4); 5, *Lanagiopollis crassa* (Van der Hammen and Wymstra, 1964) Frederiksen, 1988. Maximum diameter 62 µ.

equatorial view (slide: 1459; Coord. EF:O43 3); 6, and 7, *Lanagiopollis crassa* polar view Maximum diameter 58 µ slide: 1459; Coord. EF: S35 1); 8, *Verrutricolporites rotundiporus* Van der Hammen and Wymstra, 1964. Maximum diameter 27 µ (slide: 1461; Coord EF: R52 1; 9, *Fenestrites* sp. Maximum diameter 30 µ (slide: 1461; coord. EF: V37 3/4); 10, *Malvacipolloides maristellae* (Muller et al., 1987) Silva-Caminha et al 2010. Maximum diameter 30 µ (slide: 1461, coord. EF: M39 2); 11, *Psilastephanoporites tesseroporus* Regali et al., 1974, Maximum diameter 55 µ (slide: 1461; coord. EF: F55 3).

Fig. 15. Photomicrographs of microfossils from the Pirabas wackstone in the Atalaia outcrop. 1, *Amphistegina lessonii*; 2, *Ammonia parkinsoniana*; 3, *Elphidium sagrum*. Scale bar: 100 µm.

Fig. 16. Photomicrographs of microfossil ossicles of Echinodermata and spicules of Porifera from the Pirabas wackstone. 1.1-1.2, Comatulidae, *Sievertsella* crinoid calyx; 2.1-2.2. Comatulidae crinoid brachial ossicle; 3.1-4.3, Gorgonocephalidae ophiuroids vertebrae ossicles; 5.1-5.2, *Ophiomusium ophiuroids* vertebrae ossicle; 6.1-6.2, ophiuroids lateral arm plates; 7.1-7.2, asteroid marginal ossicles; 8.1-10.3, echinoid lantern ossicles; 11-12, Prionocidaris echinoids primary spines; 13, Echinometra echinoids primary spine; 14, Demospongiae spicule. Scale bar 20 µm (Figs. 1-4, 8-13), 40 µm (Fig. 7), 500 µm (Figs. 5-6, 14).

Fig. 17. Palaeoreconstruction of fossil assemblages recorded in the Atalaia outcrop according to the palaeoenvironment. 1. Mangrove (dark mudstone), mainly characterized by the presence of trunk and leave remains, ichnofossils and crustaceans decapods

(Microfacies C); 2. Shallow-water sandy bottom (packstone to floatstone) characterized by epifauna and infauna assemblages mostly represented by molluscs, benthic foraminifera and calcareous algae (Microfacies A). 3. Surf zone on a sandy bottom (wackstone), characterized by a high abundance of echinoderms (Microfacies B). Species identification number: 1, sea catfish Ariidae *Bagre*; 2, stingray Dasyatidae *Dasyatis*; 3, swimming crab Portunidae *Portunus*; 4, pea crab Pinnotheridae *Paleopinnixia*; 5, bighand ghost shrimp Callianassidae *Neocallichirus*; 6, box crab Calappidae *Calappa*; 7, fiddler crab Ocypodidae *Uca*; 8, Thallasinoid ichnofossil; 9, trunk and leaf; 10, eagle ray Myliobatidae *Aetobatus*; 11, great white shark Lamnidae *Carcharodon*; 12, coralline algae, *Lithotamiun*; 13, bryozoa Metrarabdotosidae *Metrarabdotus*; 14, scleractinian coral Flabellidae *Flavellus*; 15, cake urchins Clypeasteridae *Clypeaster*; 16, sea urchins Urenasteridae *Agassizia*; 17, sand dollar Clypeasteridae *Clypeaster*; 18, sea urchins Cidaridae *Prionocidaris*; 19, sea urchins Cidaridae *Cidaris*; 20, kitten´s paw clams Plicatulidae *Plicatula*; 21, clam Pectinidae *Amusium*; 22, tellins Tellinidae; 23, 25, venus clam Veneridae; 24, cockle Cardiidae; 26, spine oyster Spondylidae *Spondylus*; 27, chanks shell Turbinellidae *Turbinella*; 28, rock snails Muricidae *Murex*; 29, cowries Cypraeidae *Cypraea*; 30, top shell Calliostomatidae *Calliostoma*; 31, cone snail Conidae *Conus*; 32, spindle snail Fasciolariidae *Fusinus*; 33, dwarf olives Olivellidae *Olivella*; 34, tower snail Turritellidae *Turritella*; 35, coralline algae; 36, benthic foraminifera Amphistegenidae *Amphistegina*; 37, 39, foraminifera Spiroloculinidae *Spiroloculina*; 38, foraminifera Miliolidae *Quinqueloculina*; 40, foraminifera Hauerinidae *Pyrgo*; 41, foraminifera Rzehakinidae *Spirosigmoilinella*; 42, jack-knifefish Sciaenidae *Equetulus*; 43, nurse shark Ginglymostomatidae *Nebrius*; 44, sea lilies Comatulidae *Sievertsella*; 45, sponges Demospongea; 46, bryozoa Jaculinidae *Pirabasoporella*; 47, basket star Ophiuroidea; 48, ostracod *Bairdoppilata*.

Fig. 18. Total porosity and frequency of pores per slice on carbonate rock samples (plugs) from the Atalaia section.

Fig. 19. Total porosity and frequency of pores per slice on carbonate rock samples (plugs) from the Atalaia section (continued).

Supplementary material

S1. Microcomputer tomography (video of transaxial plane) of packstone micro plug from the Atalaia outcrop (packstone to floatstone layer at 5.0 m in the section). mp4 format, 58.2 MB, 02:18 minutes.

Credit author statement

Author contributions

OA, ACRN, RL and OOA conceived and designed the experiment. OA, AAEN, ACRN and CWM performed field trip and sample collections. OA, RL, OOA performed the experiment. OA, RL, OOA, AH, AAEN, ACRN, CWM, VTK, MVAM, GC, BBD, SAFS-C, KB and CJ analysed the information context. OA and GC wrote the paper. OA, GC, CJ, BBD, MVAM, ACRN, VTK, RL, SAFS-C and OOA revised and edited the manuscript.

Competing financial interests

The authors declare no competing interest

Highlights

1. Microfossil assemblages suggest a middle Miocene age for the uppermost Pirabas Formation at the Atalaia outcrop.
2. The palaeoenvironment are characterized by coastal lagoons with mangrove forests under the influence of a tidal regime and shallow inner platform.
3. Microfossil frameworks are responsible for the heterogeneity in the porosity values
4. The ultimate driver of the collapse of Pirabas carbonate production is still uncertaing.
5. The Pirabas Formation could become a facies model for Neogene tropical carbonate deposits of the tropical Atlantic.
6. The use of high technological resources and innovative solutions provides accurate and valuable results for micropalaeontological research

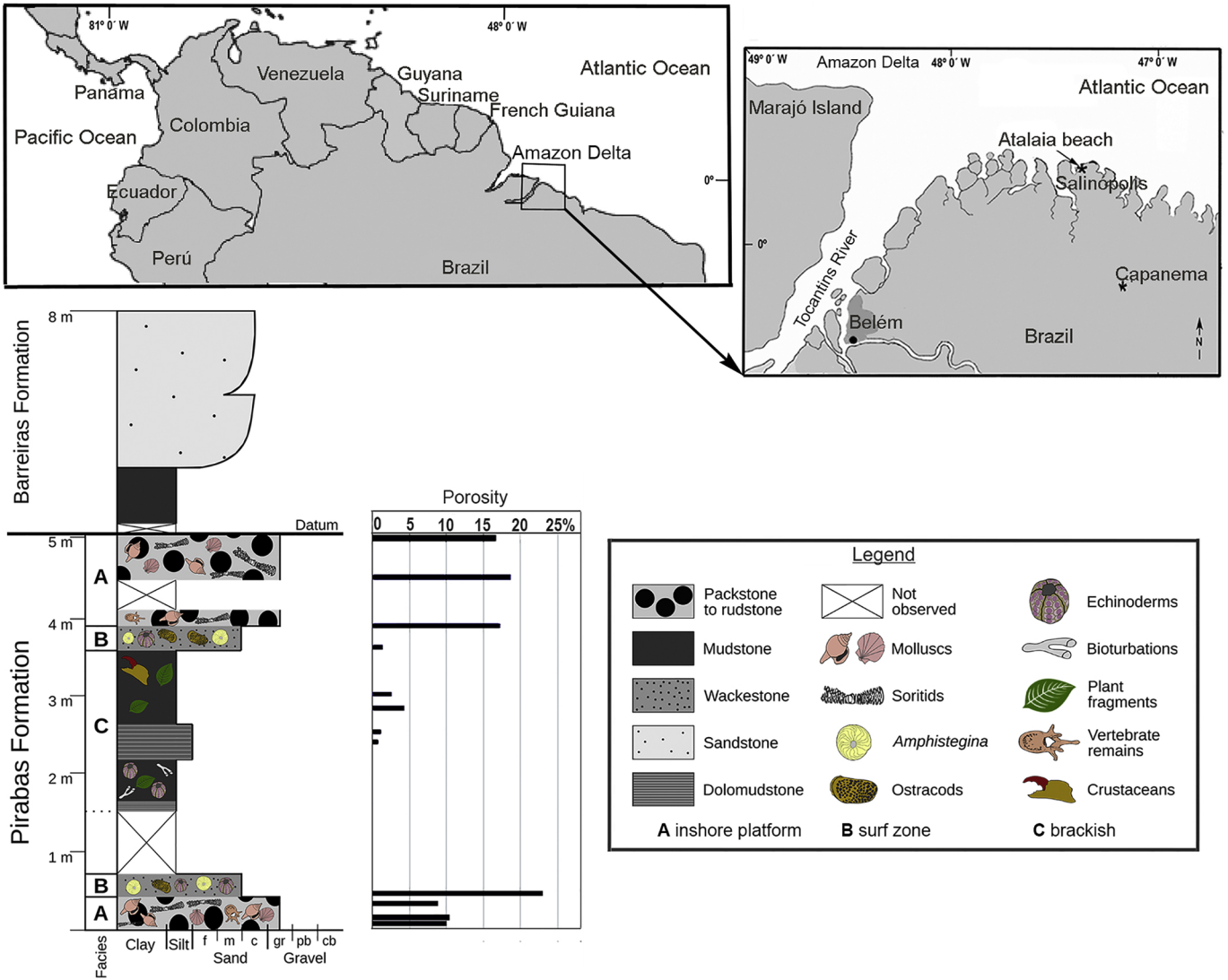
81° 0´ W
48° 0´ W
Atlantic Ocean
Panama
Venezuela
Guyana
Suriname
French Guiana
Pacific Ocean
Colombia
Amazon Delta
0°
Ecuador
Perú
Brazil
49° 0´ W
Amazon Delta
48° 0´ W
47° 0´ W
Atlantic Ocean
Marajó Island
Atalaia beach
Salinópolis
0°
Tocantins River
Capanema
Belém
Brazil
N
Barreiras Formation
8 m
Datum
Pirabas Formation
5 m
4 m
3 m
2 m
1 m
A
B
C
B
A
Facies
Clay
Silt
f
m
c
gr
pb
cb
Sand
Gravel
Porosity
0
5
10
15
20
25%
Legend
Packstone to rudstone
Not observed
Echinoderms
Mudstone
Molluscs
Bioturbations
Wackestone
Soritids
Plant fragments
Sandstone
Amphistegina
Vertebrate remains
Dolomudstone
Ostracods
Crustaceans
A inshore platform
B surf zone
C brackish

Figure 1

Figure 2

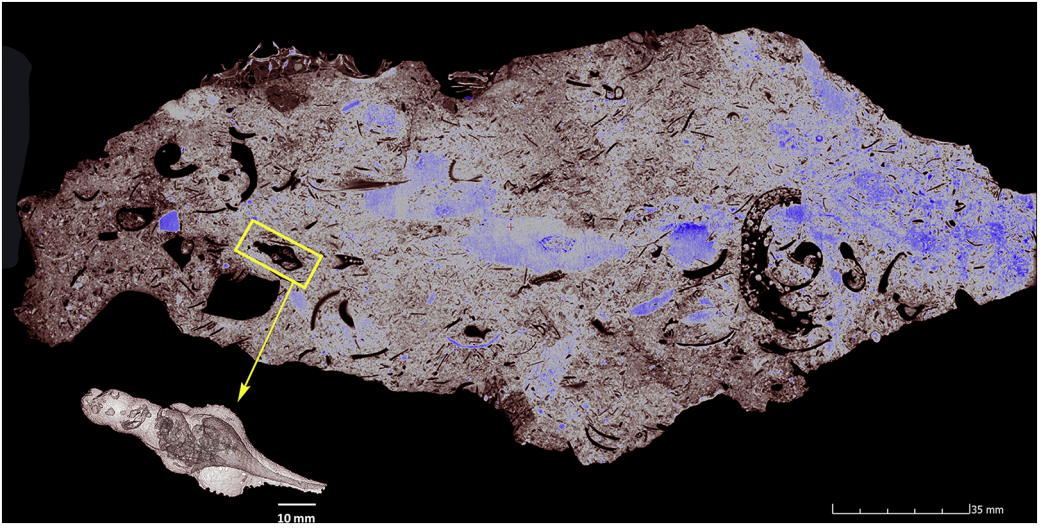

Figure 3

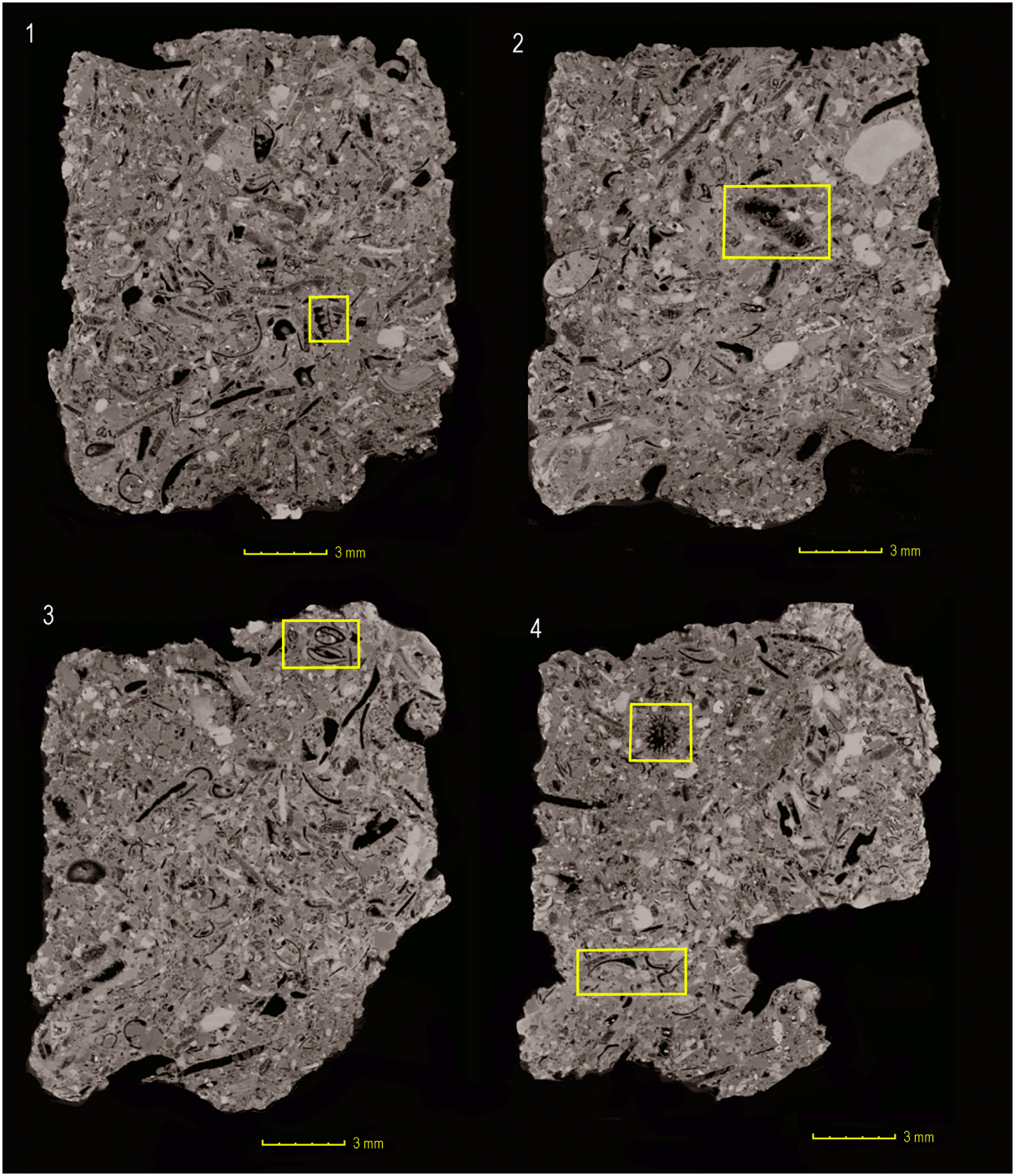

Figure 4

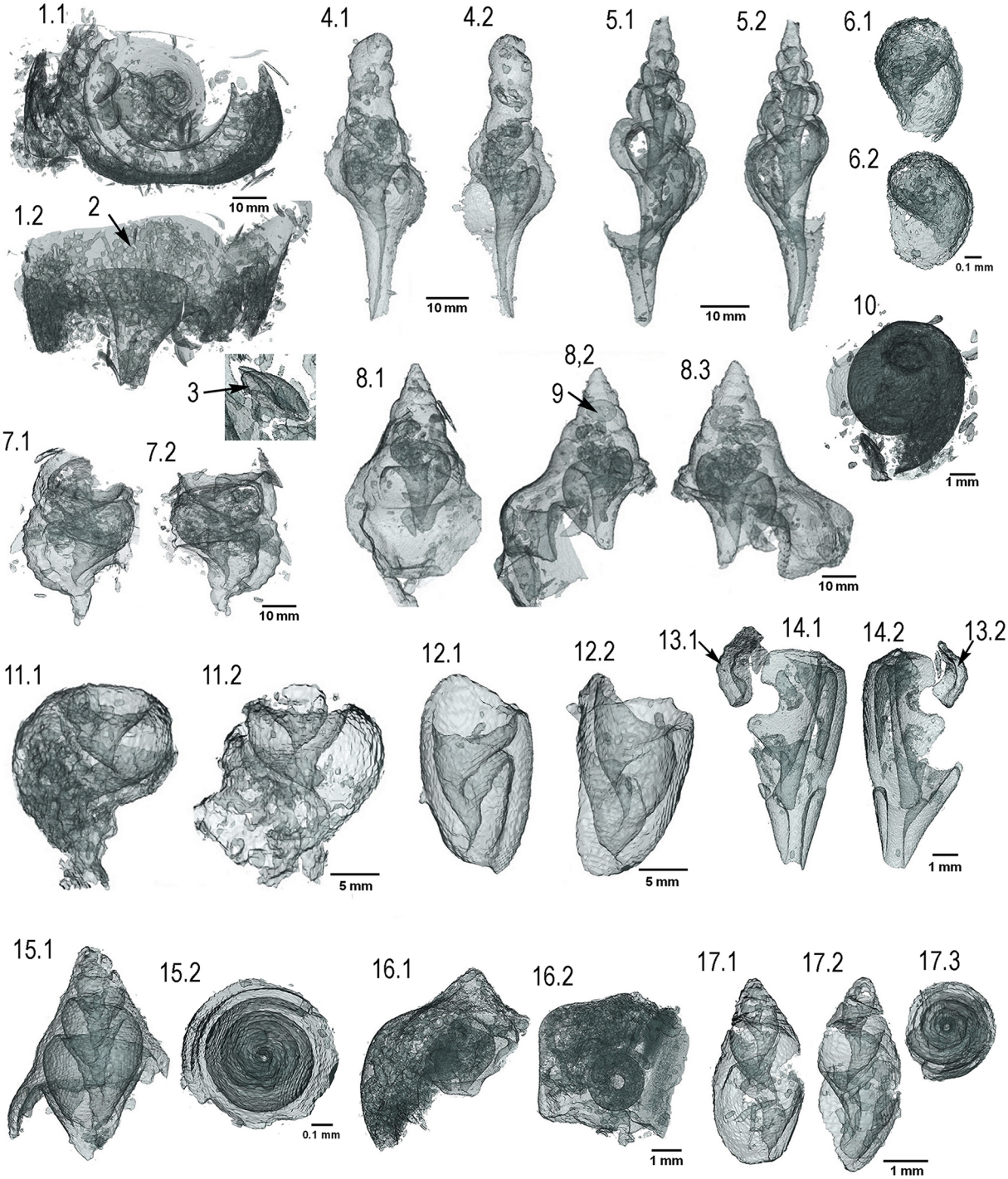
1.1
10 mm
1.2
2
3
4.1
10 mm
4.2
5.1
10 mm
5.2
6.1
6.2
0.1 mm
10
1 mm
8.1
8,2
9
8.3
10 mm
7.1
7.2
10 mm
11.1
11.2
5 mm
12.1
12.2
5 mm
13.1
14.1
14.2
13.2
1 mm
15.1
15.2
0.1 mm
16.1
16.2
1 mm
17.1
17.2
17.3
1 mm

Figure 5

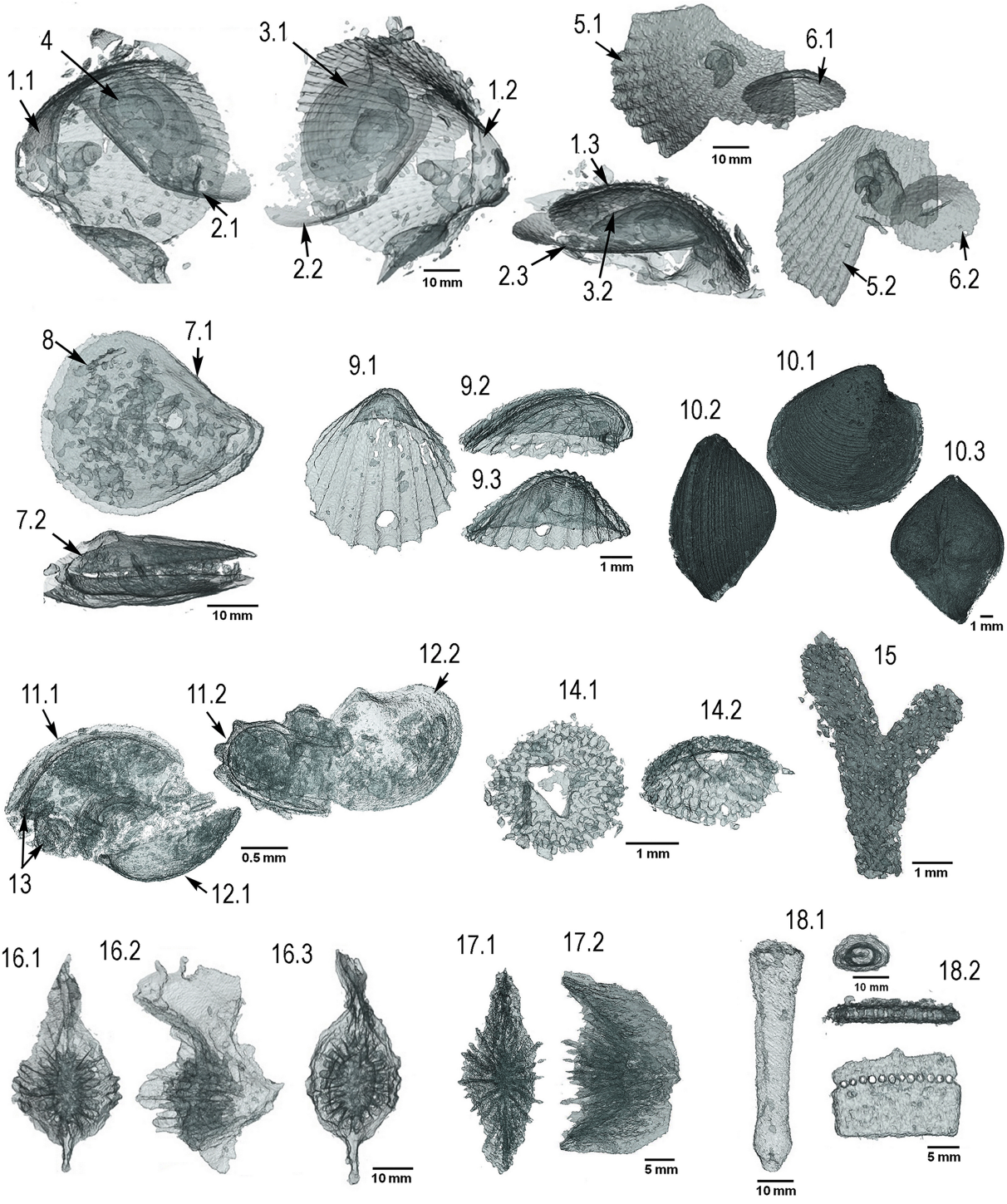
4
1.1
2.1
3.1
1.2
2.2
10 mm
5.1
6.1
10 mm
1.3
2.3
3.2
5.2
6.2
8
7.1
7.2
10 mm
9.1
9.2
9.3
1 mm
10.1
10.2
10.3
1 mm
11.1
11.2
12.2
13
12.1
0.5 mm
14.1
14.2
1 mm
15
1 mm
16.1
16.2
16.3
10 mm
17.1
17.2
5 mm
18.1
10 mm
18.2
5 mm
10 mm

Figure 6

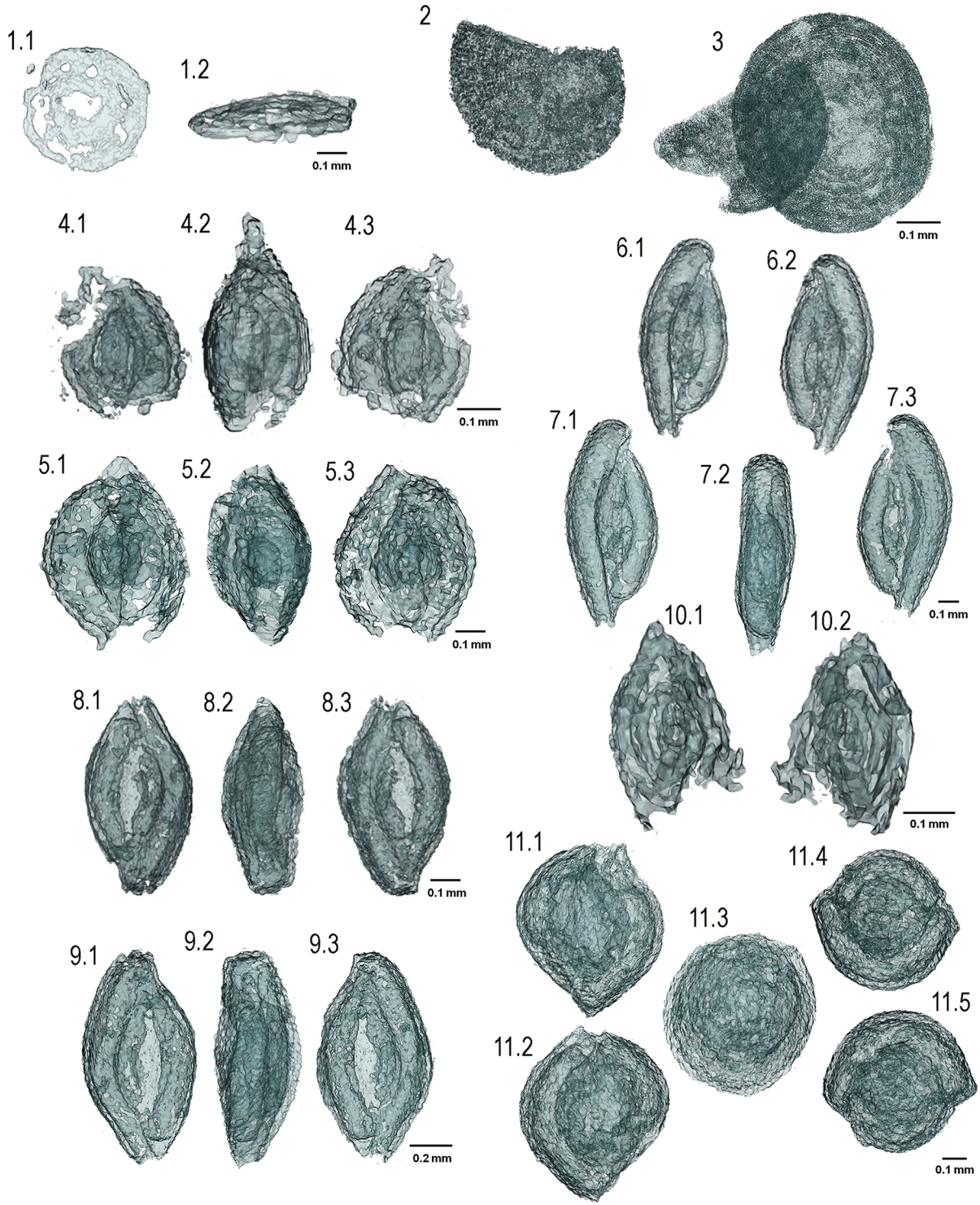
1.1
1.2
0.1 mm
2
3
0.1 mm
4.1
4.2
4.3
0.1 mm
6.1
6.2
7.1
7.2
7.3
0.1 mm
5.1
5.2
5.3
0.1 mm
10.1
10.2
0.1 mm
8.1
8.2
8.3
0.1 mm
11.1
11.4
11.3
11.5
11.2
0.1 mm
9.1
9.2
9.3
0.2 mm

Figure 7

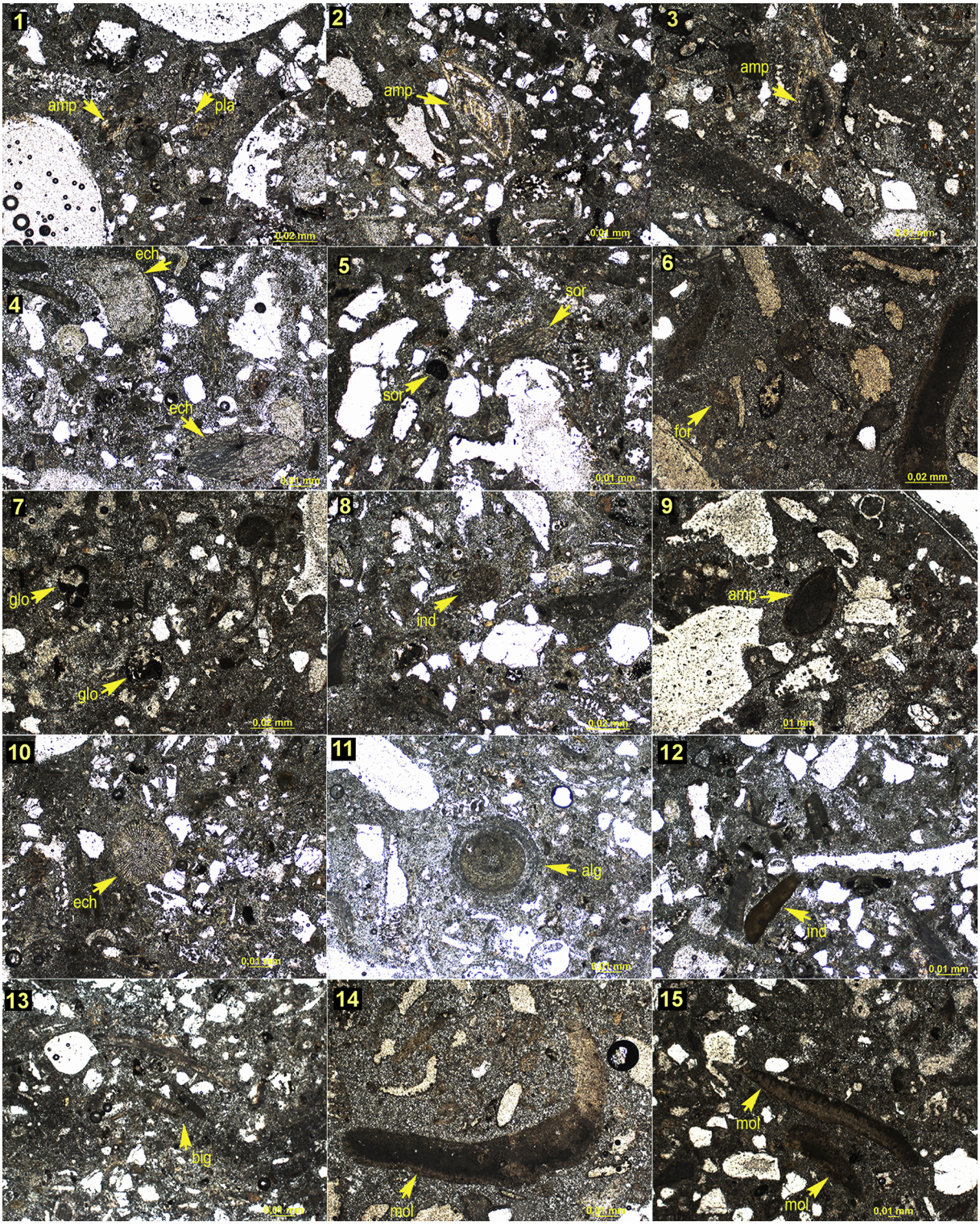
1
amp
pla
0,02 mm
2
amp
0,01 mm
3
amp
0,01 mm
4
ech
ech
0,01 mm
5
sor
sor
0,01 mm
6
for
0,02 mm
7
glo
glo
0,02 mm
8
ind
0,02 mm
9
amp
01 mm
10
ech
0,01 mm
11
alg
0,01 mm
12
ind
0,01 mm
13
big
0,01 mm
14
mol
0,01 mm
15
mol
mol
0,01 mm

Figure 8

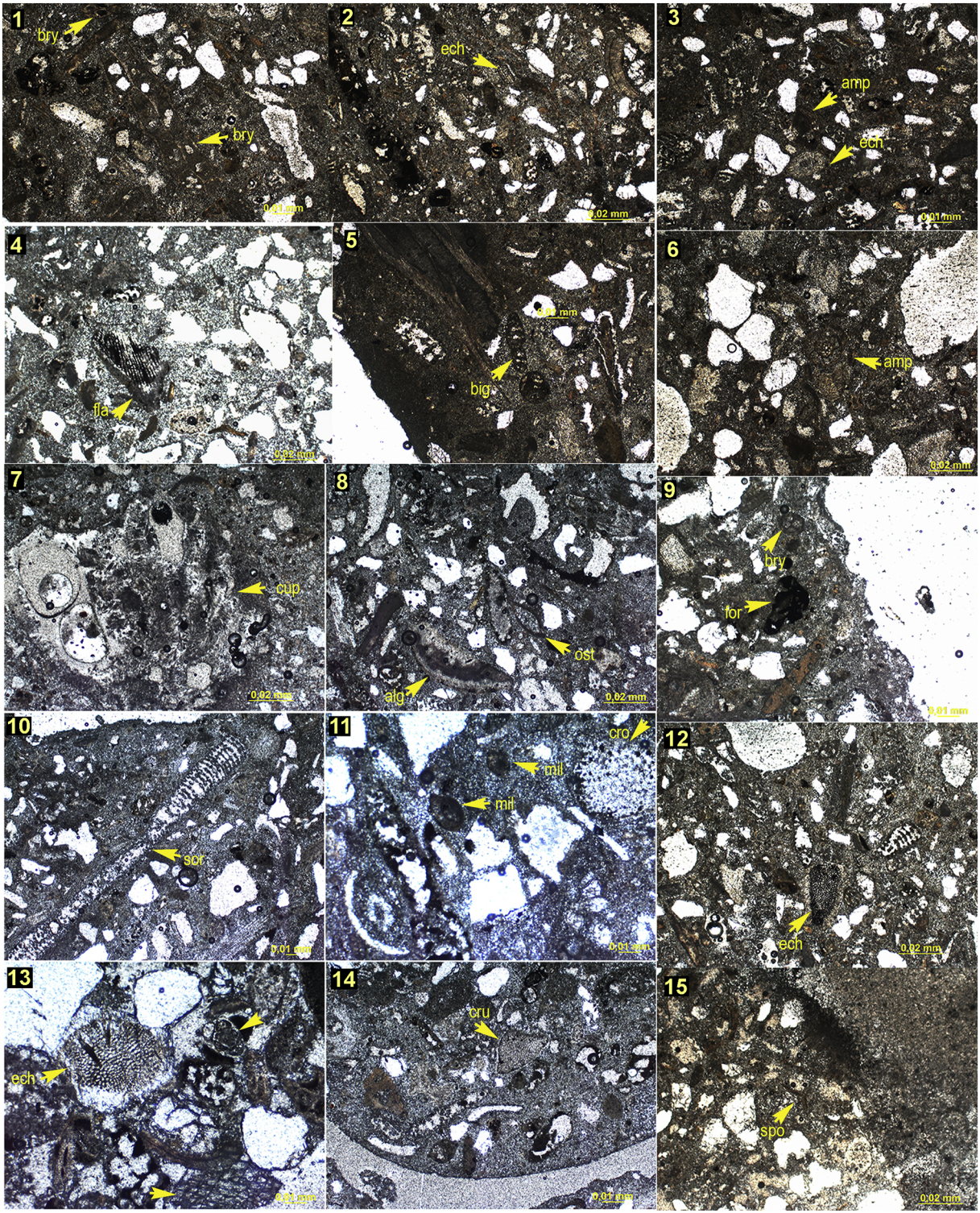
1
bry
bry
0.01 mm
2
ech
0.02 mm
3
amp
ech
0.01 mm
4
fla
0.02 mm
5
big
0.01 mm
6
amp
0.02 mm
7
cup
0.02 mm
8
ost
alg?
0.02 mm
9
bry
for
0.01 mm
10
scr
0.01 mm
11
cro
mil
mil
0.01 mm
12
ech
0.02 mm
13
ech
0.01 mm
14
cru
0.01 mm
15
spo
0.02 mm

Figure 9

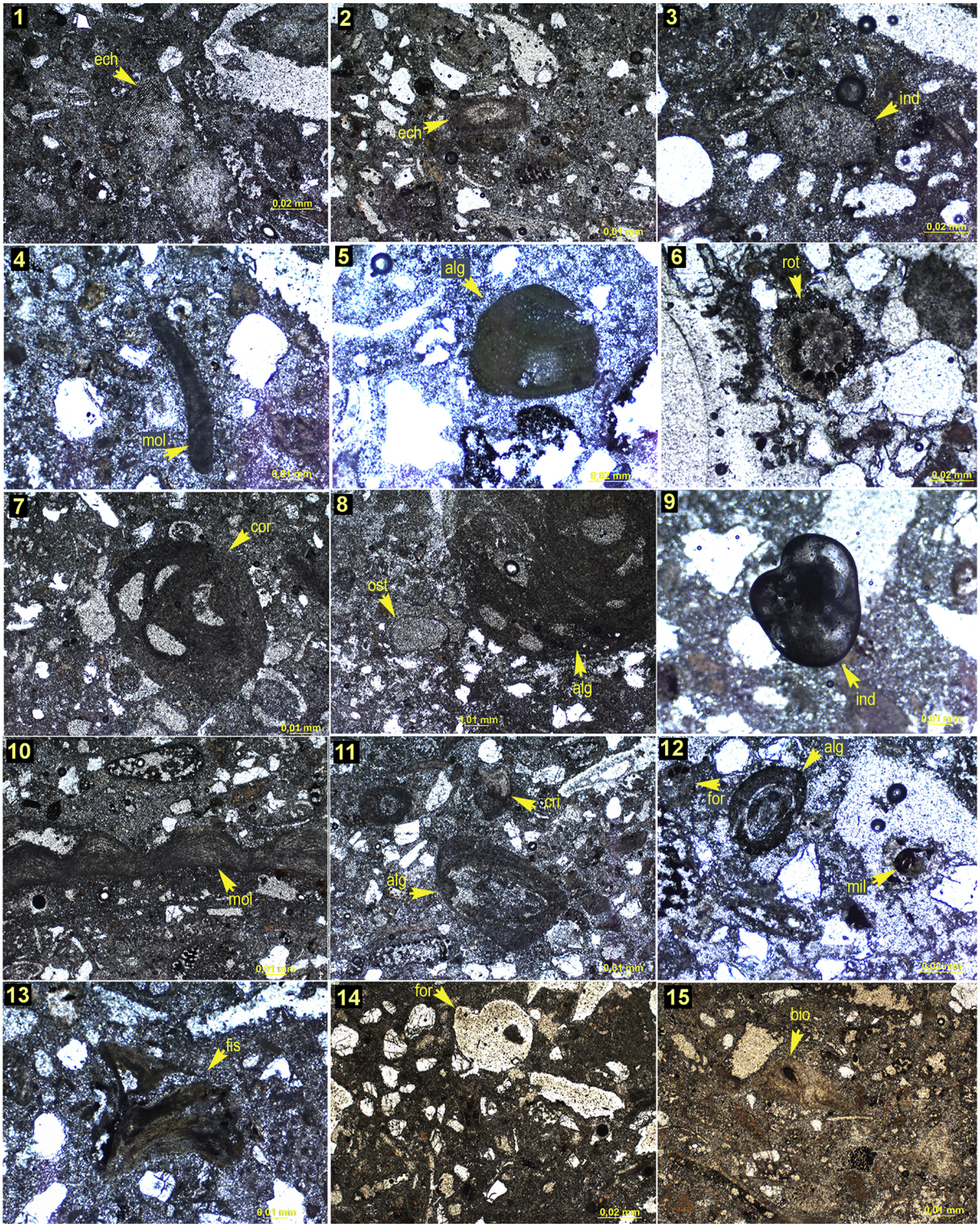
1
ech
0,02 mm
2
ech
0,01 mm
3
ind
0,02 mm
4
mol
0,01 mm
5
alg
0,02 mm
6
rot
0,02 mm
7
cor
0,01 mm
8
ost
alg
0,01 mm
9
ind
0,01 mm
10
mol
0,01 mm
11
crl
alg
0,01 mm
12
alg
for
mil
0,02 mm
13
fis
0,01 mm
14
for
0,02 mm
15
bio
0,04 mm

Figure 10

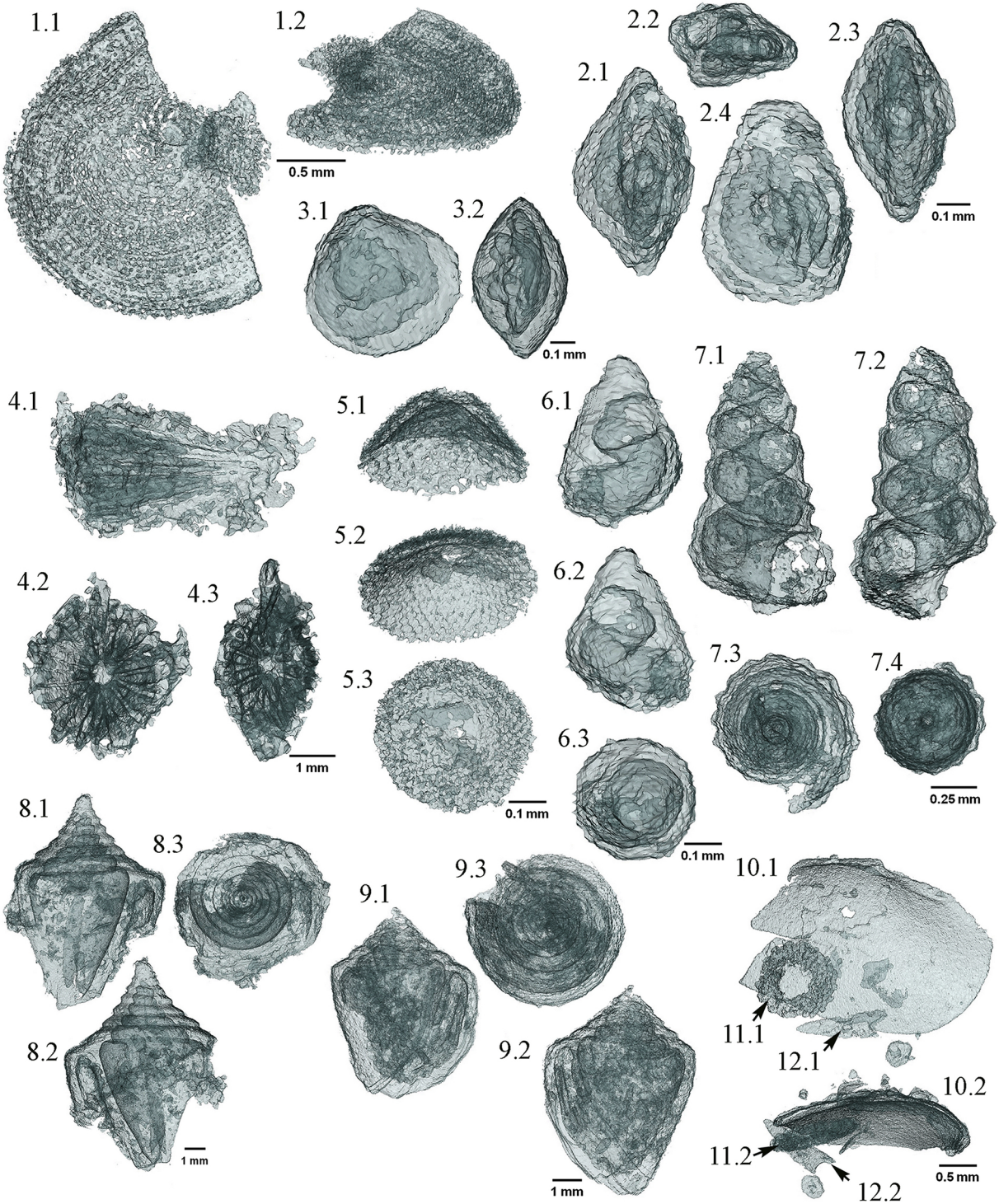
1.1
1.2
0.5 mm
2.2
2.3
2.1
2.4
0.1 mm
3.1
3.2
0.1 mm
4.1
5.1
6.1
7.1
7.2
5.2
6.2
4.2
4.3
1 mm
5.3
0.1 mm
7.3
7.4
0.25 mm
6.3
0.1 mm
8.1
8.3
9.3
9.1
10.1
11.1
12.1
8.2
1 mm
9.2
1 mm
10.2
11.2
12.2
0.5 mm

Figure 11

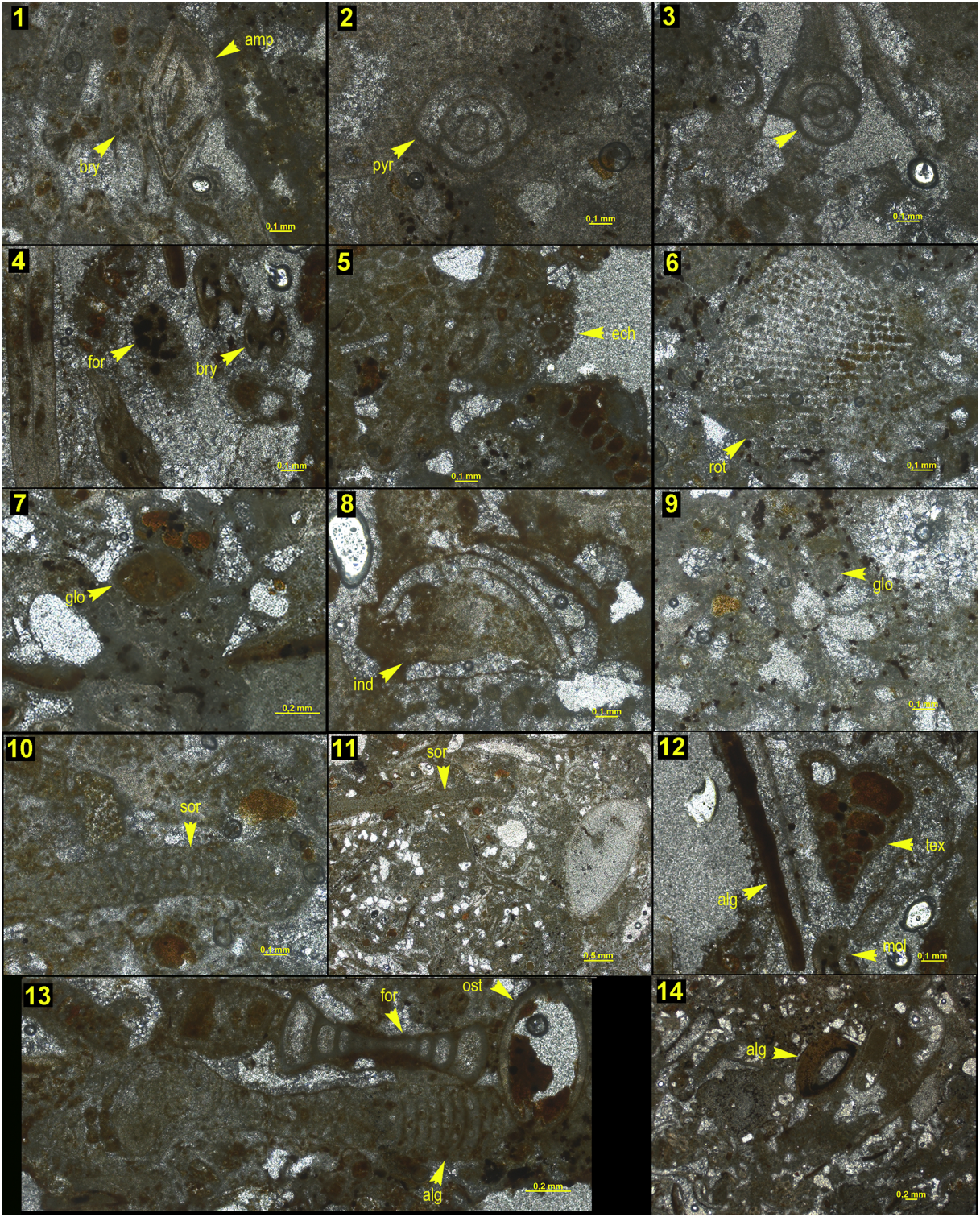
1
amp
bry
0,1 mm
2
pyr
0,1 mm
3
0,1 mm
4
for
bry
0,1 mm
5
ech
0,1 mm
6
rot
0,1 mm
7
glo
0,2 mm
8
ind
0,1 mm
9
glo
0,1 mm
10
sor
0,1 mm
11
sor
0,5 mm
12
tex
alg
mol
0,1 mm
13
for
ost
alg
0,2 mm
14
alg
0,2 mm

Figure 12

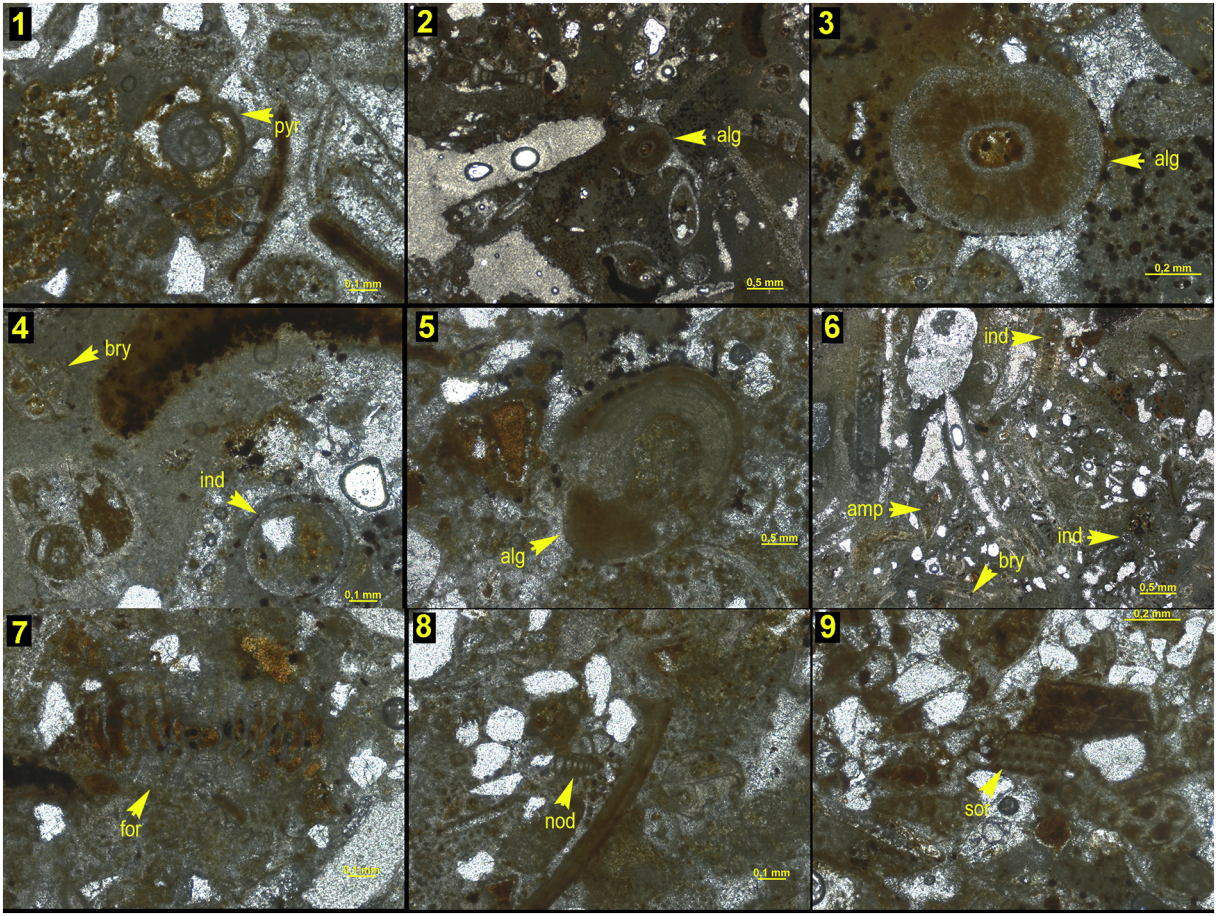
1
pyr
0,1 mm
2
alg
0,5 mm
3
alg
0,2 mm
4
bry
ind
0,1 mm
5
alg
0,5 mm
6
ind
amp
ind
bry
0,5 mm
0,2 mm
7
for
0,1 mm
8
nod
0,1 mm
9
sor

Figure 13

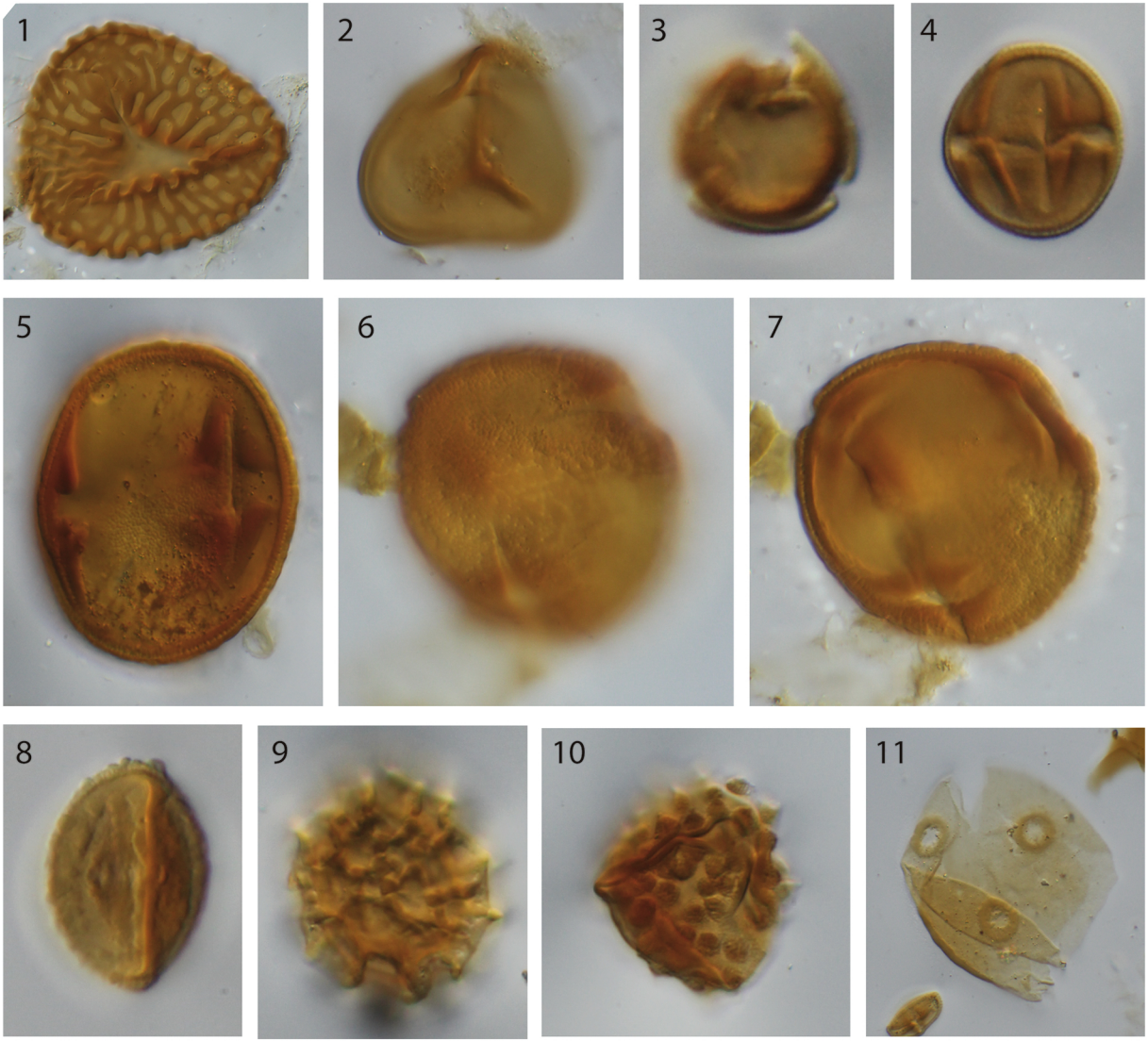

Figure 14

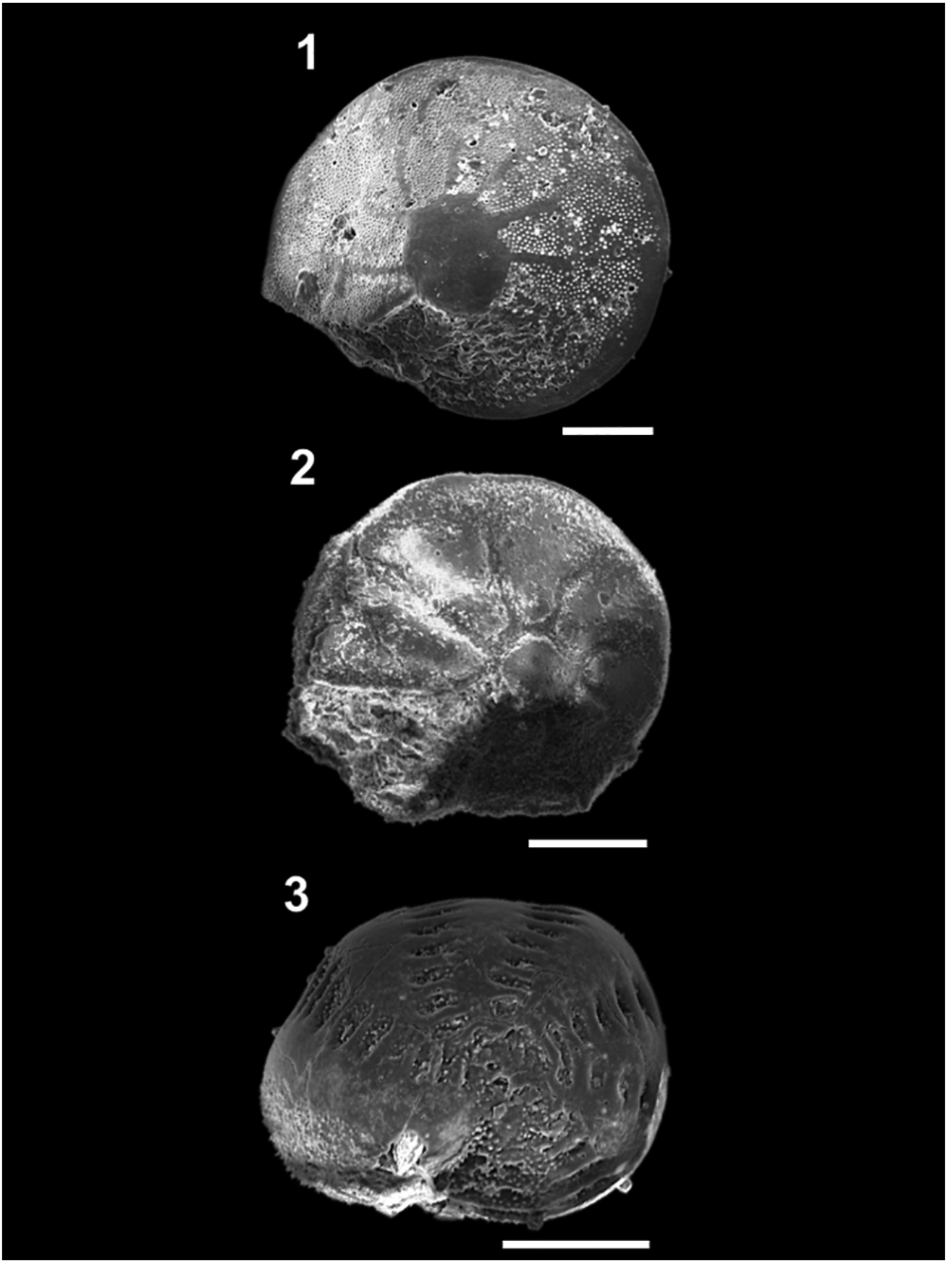

Figure 15

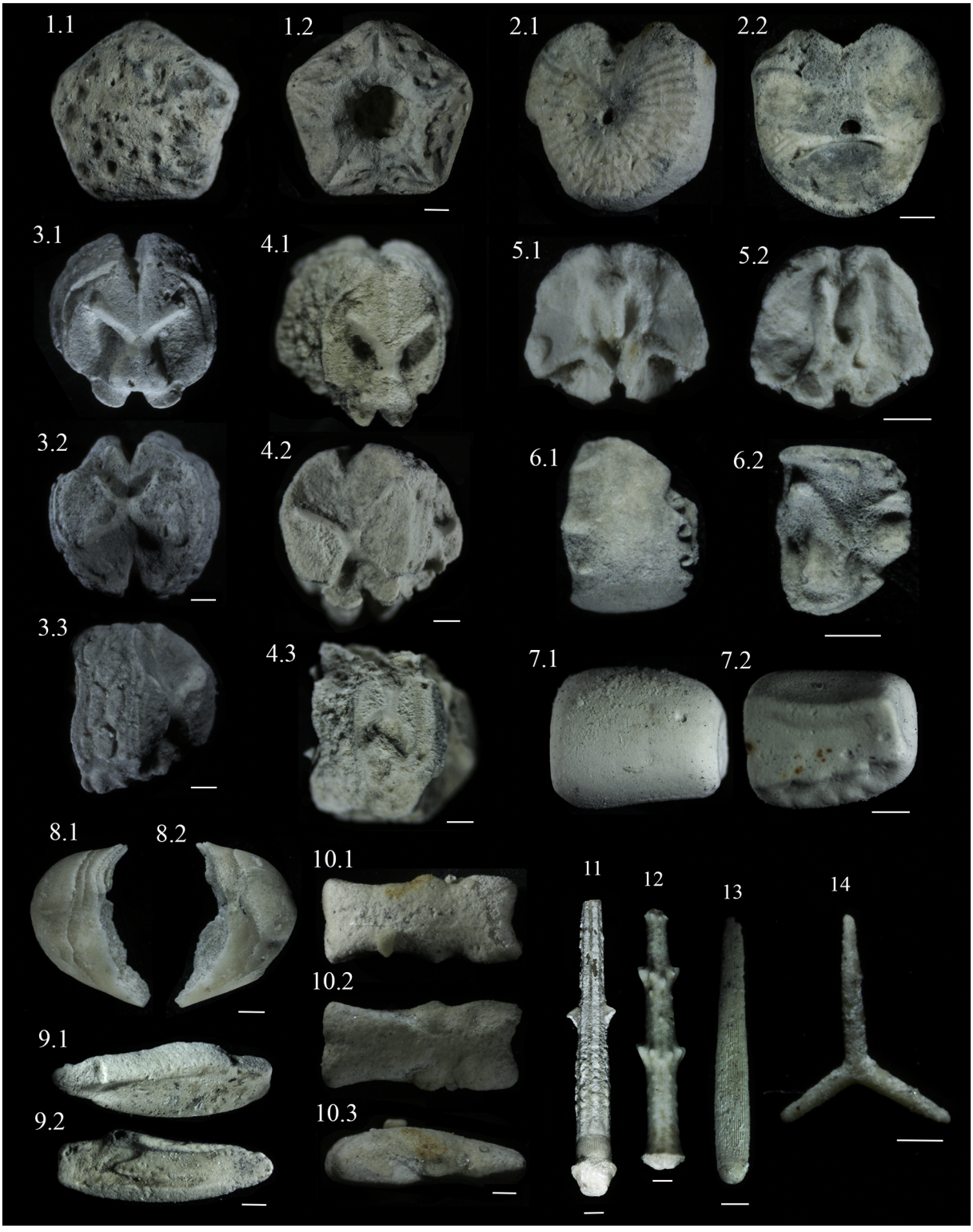
1.1
1.2
2.1
2.2
3.1
4.1
5.1
5.2
3.2
4.2
6.1
6.2
3.3
4.3
7.1
7.2
8.1
8.2
10.1
11
12
13
14
9.1
10.2
9.2
10.3

Figure 16

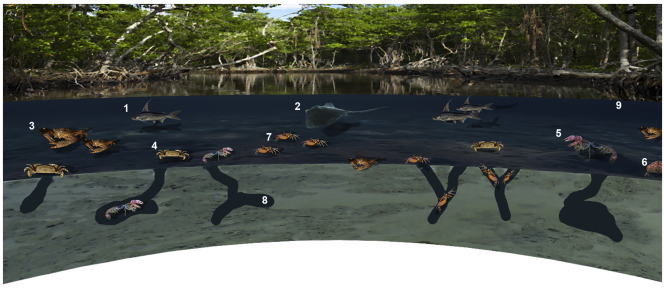
1
2
3
4
5
6
7
8
9

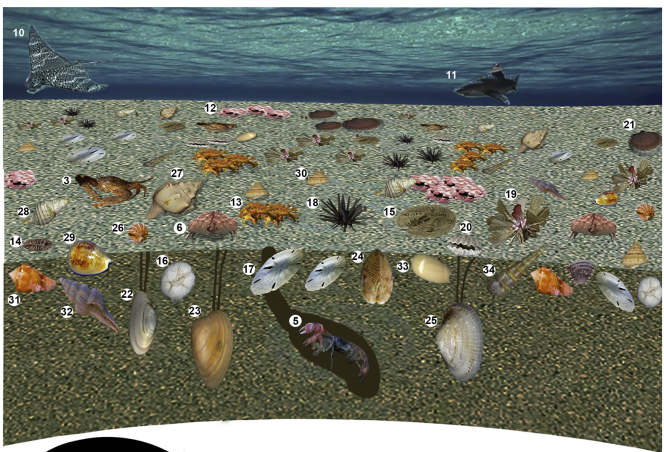
10
11
12
3
27
30
21
28
13
18
19
15
14
29
26
6
20
16
17
24
33
34
31
22
32
23
5
25


37
39
41
35
38
40
36

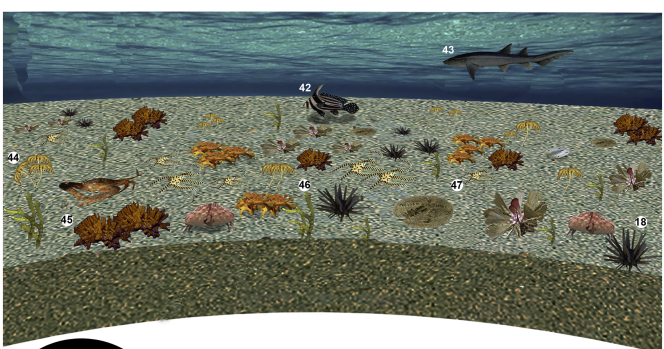
43
42
44
46
47
45
18

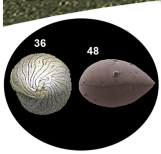
36
48

Figure 17

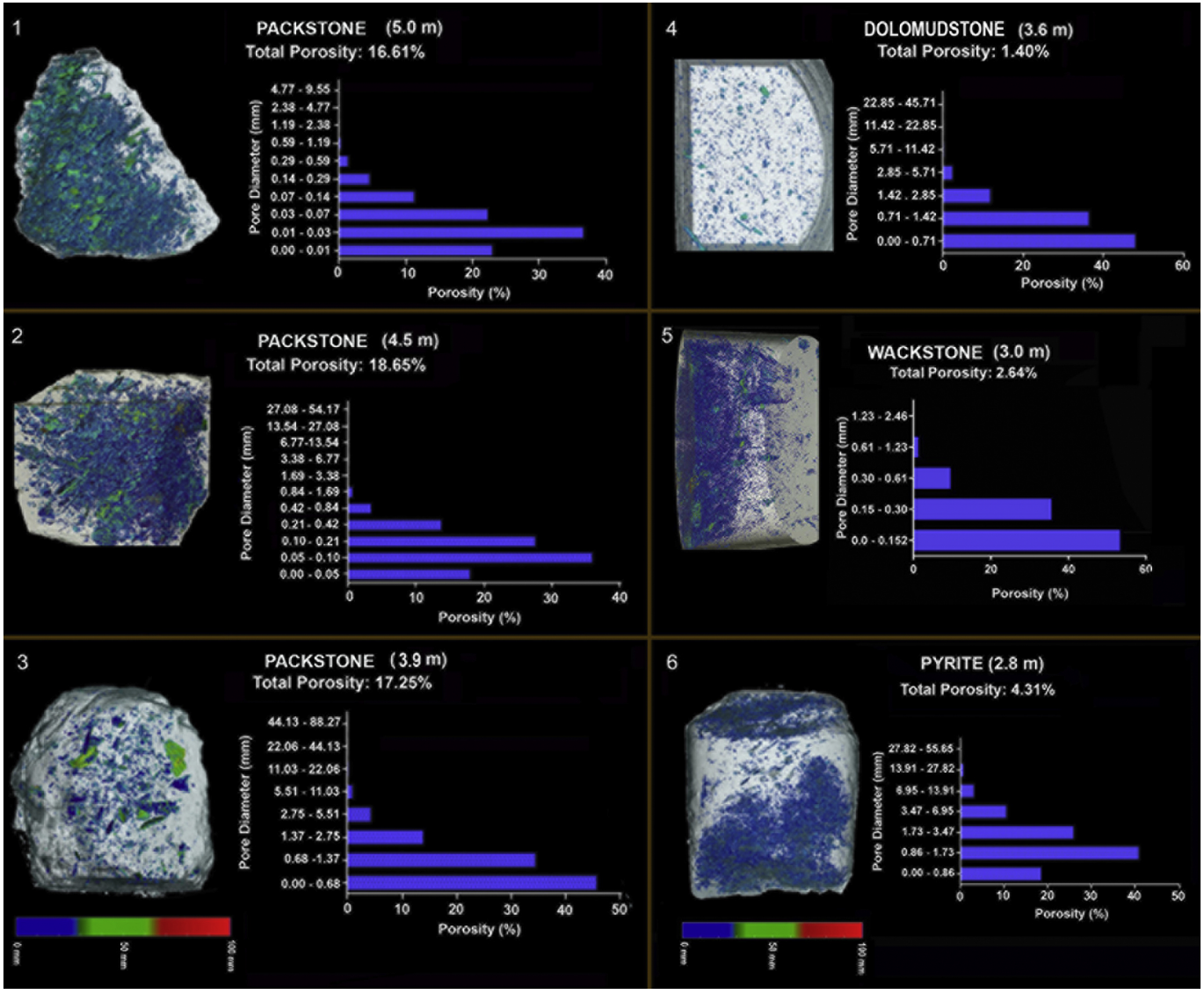
1
PACKSTONE (5.0 m)
Total Porosity: 16.61%
4.77 - 9.55
2.38 - 4.77
1.19 - 2.38
0.59 - 1.19
0.29 - 0.59
0.14 - 0.29
0.07 - 0.14
0.03 - 0.07
0.01 - 0.03
0.00 - 0.01
Pore Diameter (mm)
0 10 20 30 40
Porosity (%)
4
DOLOMUDSTONE (3.6 m)
Total Porosity: 1.40%
22.85 - 45.71
11.42 - 22.85
5.71 - 11.42
2.85 - 5.71
1.42 - 2.85
0.71 - 1.42
0.00 - 0.71
Pore Diameter (mm)
0 20 40 60
Porosity (%)
2
PACKSTONE (4.5 m)
Total Porosity: 18.65%
27.08 - 54.17
13.54 - 27.08
6.77-13.54
3.38 - 6.77
1.69 - 3.38
0.84 - 1.69
0.42 - 0.84
0.21 - 0.42
0.10 - 0.21
0.05 - 0.10
0.00 - 0.05
Pore Diameter (mm)
0 10 20 30 40
Porosity (%)
5
WACKSTONE (3.0 m)
Total Porosity: 2.64%
1.23 - 2.46
0.61 - 1.23
0.30 - 0.61
0.15 - 0.30
0.0 - 0.152
Pore Diameter (mm)
0 20 40 60
Porosity (%)
3
PACKSTONE (3.9 m)
Total Porosity: 17.25%
44.13 - 88.27
22.06 - 44.13
11.03 - 22.06
5.51 - 11.03
2.75 - 5.51
1.37 - 2.75
0.68 -1.37
0.00 - 0.68
Pore Diameter (mm)
0 10 20 30 40 50
Porosity (%)
0 mm
50 mm
100 mm
6
PYRITE (2.8 m)
Total Porosity: 4.31%
27.82 - 55.65
13.91 - 27.82
6.95 - 13.91
3.47 - 6.95
1.73 - 3.47
0.86 - 1.73
0.00 - 0.86
Pore Diameter (mm)
0 10 20 30 40 50
Porosity (%)
0 mm
50 mm
100 mm

Figure 18

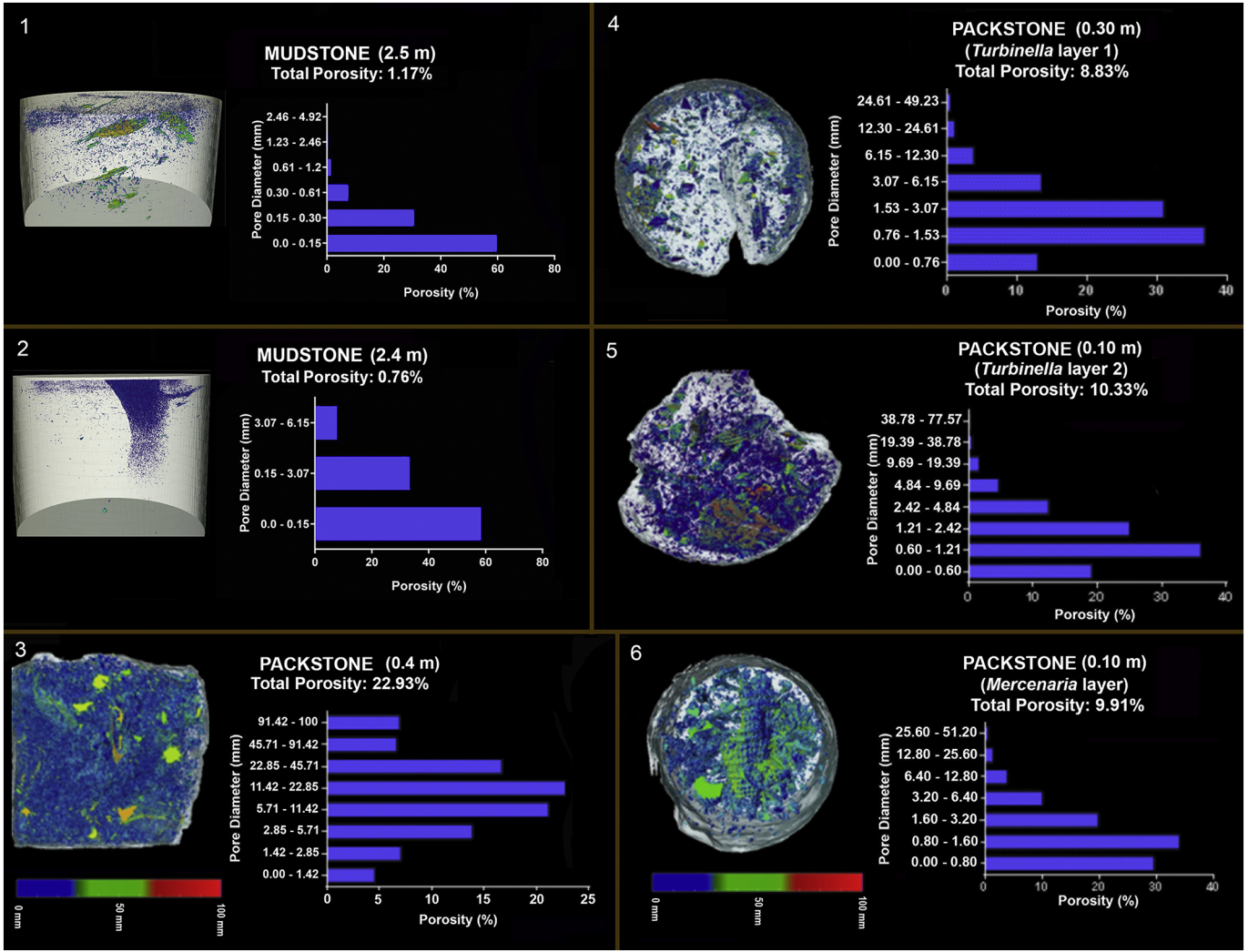
1
MUDSTONE (2.5 m)
Total Porosity: 1.17%
Pore Diameter (mm)
2.46 - 4.92
1.23 - 2.46
0.61 - 1.2
0.30 - 0.61
0.15 - 0.30
0.0 - 0.15
0
20
40
60
80
Porosity (%)
2
MUDSTONE (2.4 m)
Total Porosity: 0.76%
Pore Diameter (mm)
3.07 - 6.15
0.15 - 3.07
0.0 - 0.15
0
20
40
60
80
Porosity (%)
3
PACKSTONE (0.4 m)
Total Porosity: 22.93%
Pore Diameter (mm)
91.42 - 100
45.71 - 91.42
22.85 - 45.71
11.42 - 22.85
5.71 - 11.42
2.85 - 5.71
1.42 - 2.85
0.00 - 1.42
0
5
10
15
20
25
Porosity (%)
0 mm
50 mm
100 mm
4
PACKSTONE (0.30 m)
(Turbinella layer 1)
Total Porosity: 8.83%
Pore Diameter (mm)
24.61 - 49.23
12.30 - 24.61
6.15 - 12.30
3.07 - 6.15
1.53 - 3.07
0.76 - 1.53
0.00 - 0.76
0
10
20
30
40
Porosity (%)
5
PACKSTONE (0.10 m)
(Turbinella layer 2)
Total Porosity: 10.33%
Pore Diameter (mm)
38.78 - 77.57
19.39 - 38.78
9.69 - 19.39
4.84 - 9.69
2.42 - 4.84
1.21 - 2.42
0.60 - 1.21
0.00 - 0.60
0
10
20
30
40
Porosity (%)
6
PACKSTONE (0.10 m)
(Mercenaria layer)
Total Porosity: 9.91%
Pore Diameter (mm)
25.60 - 51.20
12.80 - 25.60
6.40 - 12.80
3.20 - 6.40
1.60 - 3.20
0.80 - 1.60
0.00 - 0.80
0
10
20
30
40
Porosity (%)
0 mm
50 mm
100 mm

Figure 19